^{230}Th and ^{231}Pa on GEOTRACES GA03, the U.S. GEOTRACES North Atlantic Transect, and implications for modern and paleoceanographic chemical fluxes

Christopher T. Hayes[a,b,*,1], Robert F. Anderson[a,b], Martin Q. Fleisher[a], Kuo-Fang Huang[c,2], Laura F. Robinson[d,e], Yanbin Lu[f], Hai Cheng[f,g], R. Lawrence Edwards[f], S. Bradley Moran[h]

[a]Lamont-Doherty Earth Observatory of Columbia University, Palisades, NY, USA

[b]Department of Earth & Environmental Sciences, Columbia University, New York, NY, USA

[c]Department of Geology & Geophysics, Woods Hole Oceanographic Institution, Woods Hole, MA, USA

[d]Department of Marine Chemistry & Geochemistry, Woods Hole Oceanographic Institution, Woods Hole, MA, USA

[e]School of Earth Sciences, University of Bristol, Bristol, United Kingdom

[f]Department of Earth Sciences, University of Minnesota, Minneapolis, MN, USA

[g]Institute of Global Environmental Change, Xi'an Jiaotong University, Xi'an, China

[h]Graduate School of Oceanography, University of Rhode Island, Narragansett, RI, USA

*corresponding author: tel: +1 (617) 324-0283, fax: +1 (617) 253-8630; Mailing address: Massachusetts Institute of Technology, Department of Earth, Atmospheric and Planetary Sciences, 45 Carleton St., E25-610,Cambridge, MA 02139, USA; Email address: cthayes@mit.edu (C. T. Hayes)

[1]Present address: Department of Earth, Atmospheric and Planetary Sciences, Massachusetts Institute of Technology, Cambridge, MA, USA

[2]Present address: Institute of Earth Sciences, Academia Sinica, Taipei, Taiwan

Keywords: GEOTRACES, North Atlantic Ocean, thorium, protactinium, scavenging, ventilation

Abstract

The long-lived uranium decay products ^{230}Th and ^{231}Pa are widely used as quantitative tracers of adsorption to sinking particles (scavenging) in the ocean by exploiting the principles of radioactive disequilibria. Because of their preservation in the Pleistocene sediment record and through largely untested assumptions about their chemical behavior in the water column, the two radionuclides have also been used as proxies for a variety of chemical fluxes in the past ocean. This includes the vertical flux of particulate matter to the seafloor, the lateral flux of insoluble elements to continental margins (boundary scavenging), and the southward flux of water out of the deep North Atlantic. In a section of unprecedented vertical and zonal resolution, the distributions of ^{230}Th and ^{231}Pa across the North Atlantic shed light on the marine cycling of these radionuclides and further inform their use as tracers of chemical flux. Enhanced scavenging intensities are observed in benthic layers of resuspended sediments on the eastern and western margins and in a hydrothermal plume emanating from the Mid-Atlantic Ridge. Boundary scavenging is clearly expressed in the water column along a transect between Mauritania and Cape Verde which is used to quantify a bias in sediment fluxes calculated using ^{230}Th-normalization and to demonstrate enhanced ^{231}Pa removal from the deep North Atlantic by this mechanism. The influence of deep ocean ventilation that leads to the southward export of ^{231}Pa is apparent. The ^{231}Pa/^{230}Th ratio, however, predominantly reflects spatial variability in scavenging intensity, complicating its applicability as a proxy for the Atlantic meridional overturning circulation.

1. Introduction

The motivations to quantify chemical fluxes in the ocean are manifold. For instance, marine biological productivity is set by the balance between nutrient sources and sinks in surface waters and global climate is influenced by the redistribution of heat and salt associated with the ocean's overturning circulation. The well-known rates of radioactive production and decay of ^{230}Th and ^{231}Pa (half-lives 75.69 kyr (Cheng et al., 2000) and 32.76 kyr (Robert et al., 1969), respectively), in addition to their insoluble nature, make them attractive tools to quantify the rates of the marine processes in which they are involved. These include removal from the water column by adsorption to particles (scavenging, related to biological productivity), redistribution by ocean circulation (related to heat transport), and sedimentation to the seafloor (providing a record of past biological productivity, ocean circulation, and more). Unfortunately, the influences of these processes on radionuclide distributions are potentially convolved. This study aims to utilize the spatial distribution of ^{230}Th and ^{231}Pa across the U.S. GEOTRACES North Atlantic Transect (Fig. 1) to characterize the modern cycling of these isotopes in an effort to more completely calibrate their use as flux tracers in the modern and past ocean.

Because their production (^{234}U and ^{235}U decay, respectively) is uniform throughout the ocean (Andersen et al., 2010; Delanghe et al., 2002; Robinson et al., 2004; Weyer et al., 2008), the key question in ^{230}Th and ^{231}Pa cycling in the water column is the balance between removal mechanisms. These are primarily (1) the downward flux by scavenging onto sinking particles and (2) lateral fluxes by advection and eddy diffusion. If lateral fluxes can be neglected, the concentration of the scavenged nuclide is expected to increase linearly with depth, representing an "equilibrium" between adsorption onto, and desorption from, vertically homogeneous sinking

particles, a concept known as reversible scavenging (Bacon and Anderson, 1982; Krishnaswami et al., 1976; Nozaki et al., 1981).

Deviations from linearity in the radionuclide profiles therefore signal where this vertical equilibrium is perturbed by lateral fluxes or where the scavenging intensity has changed. This is admittedly a simple approach, as relatively linear depth profiles are not inconsistent with some lateral flux by dispersion (Roy-Barman, 2009; Venchiarutti et al., 2008). In a basin-scale view, nonetheless, characterizing anomalies to the predictions of reversible scavenging is our first step in deconvolving the oceanic ^{230}Th and ^{231}Pa cycles. Three such anomalies, boundary scavenging, the effects of recently ventilated deep water, and bottom scavenging, appear in unprecedented detail in our North Atlantic section (Fig. 1). We now provide a context for these findings.

1.1 Boundary scavenging of ^{230}Th and ^{231}Pa

Boundary scavenging (Bacon, 1988; Bacon et al., 1976; Spencer et al., 1981) is the enhanced removal of scavenged-type elements (Bruland and Lohan, 2003) at ocean margins. When lateral gradients in particle flux exist, as between biologically productive ocean margin regions and oligotrophic ocean interior regions, insoluble elements are removed from the water column by scavenging to a greater extent at the margin versus the interior. The resulting gradient in radionuclide concentration produces a dispersive flux toward the margin from the interior. Lateral transport in the water column toward ocean margins is more significant for ^{231}Pa than for ^{230}Th because it is more slowly removed downward by scavenging. The residence time with respect to scavenging of ^{231}Pa is 50-200 yrs while that for ^{230}Th is 10-40 yrs (Henderson and Anderson, 2003). On the basis of the boundary scavenging concept alone, elevated ^{231}Pa/^{230}Th ratios in both the dissolved and particulate phase at ocean margins are expected (Fig. 2). Prior to this study, the lateral gradients in the dissolved ^{231}Pa/^{230}Th ratio or in dissolved ^{230}Th (^{231}Pa) concentrations,

predicted by the boundary scavenging concept, have not been definitively observed in the North Atlantic.

Modeling efforts have concluded that in ~70% of the ocean, ^{230}Th is redistributed laterally by no more than 30% of its in situ production in the water column (Henderson et al., 1999), consistent with available observations from sediment traps (Yu et al., 2001). However, on the basis of sedimentary records some authors have argued that water column ^{230}Th redistribution could be much greater than 30% due to boundary scavenging-type mechanisms, specifically along the equator in the Pacific (Broecker, 2008; Lyle et al., 2005; Lyle et al., 2007). This claim derives from a concern regarding ^{230}Th-normalization, a method for calculating sediment accumulation rates on the basis of sedimentary ^{230}Th concentrations (Bacon, 1984; François et al., 2004). This method assumes that the burial flux of ^{230}Th is equal to its rate of production by ^{234}U decay in the overlying water column, which allows one to correct for the lateral redistribution of sediments at the seafloor (sediment focusing). Because glacial-interglacial changes in sediment focusing have enhanced or diminished apparent accumulation rates by more than a factor of 2 (François et al., 1990; Suman and Bacon, 1989), the approach has been defended on the basis that neglecting a relatively small bias in the assumption that ^{230}Th burial is equivalent to its production in the overlying water column is justified (François et al., 2007; Siddall et al., 2008). One aim of this study is to quantitatively estimate the magnitude of ^{230}Th redistribution due to boundary scavenging.

While the effect of boundary scavenging of ^{231}Pa is well-expressed in the Pacific (Anderson et al., 1983; Anderson et al., 1990; Walter et al., 1999; Yang et al., 1986), it is considered to be suppressed in the Atlantic. This is because this basin is ventilated by southward flowing North Atlantic Deep Water (NADW) on timescales (<100-200 yrs) (Broecker et al., 1991) shorter than

the Pa residence time with respect to scavenging (Walter et al., 1999; Yu et al., 1996; Yu et al., 2001). This means Pa can be transported south by deep water flow before it can be dispersed to North Atlantic margins. Although some studies have found evidence, in the form of sedimentary $^{231}Pa/^{230}Th$ activity ratios above that produced in seawater by uranium decay of 0.093, for the enhanced removal of ^{231}Pa in the upwelling area off Northwest Africa (Legeleux et al., 1995; Lippold et al., 2012b; Mangini and Diester-Haas, 1983), studies of the North American (Anderson et al., 1994; Lippold et al., 2012a) and the northern Brazil (Lippold et al., 2011) margins do not support boundary scavenging of Pa. The dissolved $^{231}Pa/^{230}Th$ distribution toward the margins of our transect (Fig. 1) will be used to determine the significance of boundary scavenging in the North Atlantic in light of its recent ventilation.

1.2 The impact of Atlantic circulation

The possibility of boundary scavenging notwithstanding, previous studies have demonstrated that deepwater distributions of ^{230}Th and ^{231}Pa are significantly perturbed by the influence of the recent ventilation of NADW (Luo et al., 2010; Moran et al., 1997; Moran et al., 1995; Moran et al., 2002; Scholten et al., 2001; Vogler et al., 1998). Deep convection at sites of deep water formation results in the injection to depth and propagation along deepwater flow paths of ^{231}Pa and ^{230}Th concentrations which are lower than predicted by reversible scavenging (Moran et al., 1997; Moran et al., 1995; Moran et al., 2002). As the water mass ages, isolated from further perturbations to scavenging equilibrium, dissolved ^{230}Th concentrations increase due to exchange with sinking particles, reaching a steady-state distribution relatively rapidly (determined by the residence time of 10-40 yrs), while ^{231}Pa responds more slowly (residence time of 50-200 yrs) because of the differing scavenging rates of the two elements (Moran et al., 2001; Rutgers v. d. Loeff and Berger, 1993). The longer residence time of ^{231}Pa allows for its southward export with

NADW, leaving a ^{231}Pa deficit in deep North Atlantic sediments (Yu et al., 1996). This is the basis for using the sedimentary $^{231}Pa/^{230}Th$ ratio as an indicator of the strength of the Atlantic meridional overturning circulation (McManus et al., 2004). The present water column transect is also intended to document the impact of ventilation on ^{231}Pa and the $^{231}Pa/^{230}Th$ ratio.

In the absence of variations in scavenging intensity, one expects ^{230}Th and ^{231}Pa concentrations and the $^{231}Pa/^{230}Th$ ratio to increase with water mass age or time since deep water formation. The strongest response to ageing occurs within 1 to 2 water column residence times after deep water formation. Our section is appropriate to test this prediction because deep water age, or the time since deep-water (as averaged below 2 km) has been isolated from the atmosphere, ranges from <50 yrs in the west to >250 yrs in the east (Broecker et al., 1991). We have extracted an estimate of mean age for our North Atlantic transect from a recent inversion of ventilation tracer observations (^{14}C, CFCs, PO_4^*, temperature and salinity) by Khatiwala et al. (2012). These ventilation ages, which represent the time since a water parcel was last at the surface, taking into account contributions from multiple pathways and source regions, are referred to in the text as mean ages.

In addition to consideration of water mass ageing, we put our transect into hydrographic context with the salinity and neutral density (γ_n) section in Fig. 1. The dome of salty subtropical mode water, also known as Eighteen Degree Water, is apparent in the upper 500-800 m and is roughly bound at depth by γ_n = 26.65 kg m^{-3} (LeBel et al., 2008). The remaining density surfaces in Fig. 1 demarcate the boundaries between the various sources of NADW, which are defined most clearly in the Northwest section between Bermuda and Woods Hole, Mass., known as Line W (Toole et al., 2011). These are, in order of increasing density, Upper and Classic Labrador Sea Water, Iceland-Scotland Overflow Water, and Denmark-Strait Overflow Water, which is underlain

by Antarctic Bottom Water (AABW, γ_n > 28.125). While we name the densest layer of water in the western basin AABW, this water mass, far from its source, must have gone through significant mixing with the overlaying NADW.

The deep waters of the Northeastern Atlantic (>3 km depth) are not as clearly defined by the contributions to NADW and are characterized by a relatively homogeneous water mass called Northeast Atlantic Deep Water (NEADW). NEADW is sourced by a mixture of NADW and AABW which enters the Northeast basin largely through the Vema Fracture Zone at 11°N (McCartney et al., 1991), with some contribution from the Romanche Trench near the equator (Broecker et al., 1980; Schlitzer, 1987; Schlitzer et al., 1985). The intermediate water in the southeastern portion of the cruise track intersects the northern extent of the salinity minimum (and silicic acid maximum) originating from Antarctic Intermediate Water (AAIW) (Talley, 1999; Tsuchiya, 1989), outlined in Fig. 1. Lastly, the high salinity intrusion of Mediterranean Outflow Water (MOW) at ~1 km depth is well represented on the largely south-north part of the transect approaching Portugal.

1.3 Bottom scavenging

Deep water ^{231}Pa and ^{230}Th concentrations can also be perturbed by changes in scavenging intensity near the seafloor (bottom scavenging) associated with a change in particle concentration or particle composition. Nepheloid layers (Biscaye and Eittreim, 1977; McCave, 1986), or zones up to hundreds of meters above the seafloor of increased particle concentration caused by the resuspension of sediments, have been known to enhance the scavenging of the shorter-lived ^{234}Th (half-life 24.1 days) in the northwest (Bacon and Rutgers v. d. Loeff, 1989; DeMaster et al., 1991) and northeast (Schmidt, 2006; Turnewitsch et al., 2008; Turnewitsch and Springer, 2001) Atlantic. Previous studies in the North Atlantic have suggested that bottom scavenging could reduce the

186 ^{230}Th concentration in deep water, but since the same effect can be achieved via recent water mass
187 ventilation without invoking a change in scavenging intensity, ventilation was the preferred
188 explanation (Moran et al., 1997; Moran et al., 1995; Vogler et al., 1998). However, recent results
189 from the Pacific, where the ventilation effect is not large enough to produce observed radionuclide
190 depletions in deepwater, have confirmed early observations (Bacon and Anderson, 1982; Nozaki
191 and Nakanishi, 1985) that significant bottom scavenging indeed occurs for ^{230}Th (Hayes et al.,
192 2013; Okubo et al., 2012; Singh et al., 2013) and ^{231}Pa (Hayes et al., 2013). Furthermore, nepheloid
193 layers in the South Atlantic have been found to significantly enhance scavenging of ^{230}Th and ^{231}Pa
194 (Deng et al., 2014).

195 Based on extensive observations in the northwest Atlantic of thick nepheloid layers
196 (Biscaye and Eittreim, 1977; Brewer et al., 1976), our transect is well situated to determine the
197 effect of sediment resuspension on ^{230}Th and ^{231}Pa. In addition to increased particle loading,
198 bottom scavenging may also be affected by a change in particle composition. This section is also
199 well suited to test the hypotheses that ^{230}Th and ^{231}Pa are scavenged especially efficiently by
200 authigenic iron and manganese oxide phases associated with hydrothermal activity at the mid-
201 Atlantic ridge (German et al., 1991; German et al., 1993) or by (oxy)hydroxide coatings of particles
202 formed in regions of organic-rich sediment diagenesis at ocean margins (Anderson et al., 1983;
203 Bacon et al., 1976; Shimmield et al., 1986). To infer likely changes in scavenging intensity in our
204 transect, we utilize the distribution of the particle beam attenuation coefficient, C_p, as measured
205 by transmissometer from CTD casts, which is, to first order, linearly related to particle
206 concentration (Bishop, 1986; Gardner et al., 1985), although the sensitivity of C_p to particle
207 concentration is known to vary with particle size and composition (Baker and Lavelle, 1984;
208 Richardson, 1987).

2. Methods

The U.S. Geotraces North Atlantic transect (Fig. 1) consisted of two legs, collectively designated GA03 in the global GEOTRACES survey (geotraces.org). KN199-4 (referred to as GT10) from Lisbon, Portugal to Mindelo, Cape Verde was completed in Oct-Nov 2010. KN204-1 (referred to as GT11) from Woods Hole, Massachusetts to Praia, Cape Verde via St. Georges, Bermuda was completed in Nov-Dec 2011. Radionuclide data were produced by three collaborating laboratories which were intercalibrated (Anderson et al., 2012) to analyze dissolved (<0.45 µm) and particulate (0.45-51 µm) ^{232}Th, ^{230}Th, and ^{231}Pa in seawater: the Lamont-Doherty Earth Observatory of Columbia University (L-DEO), the Woods Hole Oceanographic Institution (WHOI) and the University of Minnesota (UMN). Five liter water samples were collected using conventional Niskin bottles, filtered with 0.45 µm Acropak^{TM}-500 filter capsules, and acidified to pH = 1.8 at sea for storage according GEOTRACES protocols. Particulate samples representing 55-350 L of seawater were collected by McLane Research in situ pumps with a redesigned filter holder (Lam and Morris, 2013) using paired 0.8 µm Pall Supor800 polyethersulfone filters (Bishop et al., 2012).

Th and Pa isotopes (including the added tracers ^{229}Th and ^{233}Pa) were co-precipitated with Fe (oxy)hydroxide for pre-concentration and purification using acid digestions (HNO_3/HF/$HClO_4$, depending on the laboratory) and ion exchange chromatography. Filter samples were co-precipitated with Fe after complete dissolution (HNO_3/$HClO_4$/HF). Radionuclide concentrations were determined by isotope dilution inductively-coupled plasma mass spectrometry. We converted radionuclide mass concentrations to radioactivity units using the conversion factors, 0.7591 µBq/fg ^{230}Th and 1.7476 µBq/fg ^{231}Pa. The analytical procedures used at L-DEO, WHOI, and

231 UMN have been fully described by Anderson et al. (2012), Auro et al. (2012), and Shen et al.
232 (Shen et al., 2003; Shen et al., 2002; Shen et al., 2012), respectively.

233 We correct measured dissolved radionuclide concentrations for in-growth due to uranium
234 decay during sample storage (Robinson et al., 2004). In-growth during sample storage from
235 particulate U concentrations is negligible (Anderson, 1982). In order to isolate the signature of
236 scavenging in the dissolved phase we also correct ^{230}Th and ^{231}Pa concentrations for a contribution
237 produced by the partial dissolution of U-containing lithogenic material based on dissolved ^{232}Th
238 as described by Hayes et al. (2013), assuming a crustal ^{238}U/^{232}Th ratio and congruent dissolution
239 of ^{232}Th, ^{230}Th and ^{231}Pa. Similarly, in the particulate phase we correct measured ^{230}Th and ^{231}Pa
240 for a lithogenic component based on particulate ^{232}Th. All radionuclide concentrations discussed
241 in the text are corrected for lithogenic sources and are denoted as "xs". For more information on
242 data analysis see the metadata associated with these data online (http://www.bco-
243 dmo.org/dataset/3847 or http://www.bodc.ac.uk/geotraces/data/). Forthcoming studies will
244 present and interpret the distribution of ^{232}Th and particulate radionuclides in their own right.
245 These results are used here only for the interpretation of the dissolved (or total) ^{230}Th and ^{231}Pa
246 distributions.

247 **3. Results and Discussion**

248 *3.1 Sections of dissolved ^{230}Th xs and ^{231}Pa xs*

249 Deviations from linear concentration-depth profiles as predicted by the model of reversible
250 scavenging are immediately apparent in the North Atlantic sections (Fig. 3). Both radionuclides
251 display substantial lateral concentration gradients, some of which are clearly related to recent
252 ventilation. Generally, lower concentrations of both radionuclides are found in the western and
253 northern parts of the transect, coincident with younger mean ages (Fig 3E). Additionally low

concentrations of ^{231}Pa xs in shallow water (Fig. 3D) take on a dome structure, coinciding with EDW, and are presumably reflective of the rapid (<10 yrs) ventilation of this subtropical mode water (Jenkins, 1988).

Notably unrelated to any change in mean age (Fig. 3E), ^{230}Th xs also has reduced concentrations throughout the water column in the section between Cape Verde and Mauritania (Cape Verde transect, Fig. 3B) coincident with increasing particle concentrations (Fig 3A, 5000-6500 km section distance). The plunging isolines of ^{230}Th xs concentration toward the continental margin on this transect are strong evidence for the process of boundary scavenging occurring. We quantify the lateral transport of ^{230}Th xs and ^{231}Pa xs associated with this boundary scavenging in section 3.2.

Both radionuclides show vertical concentration anomalies as well. Concentrations generally increase linearly from the surface to depth but nearly always begin to decrease toward the seafloor. These negative deviations with respect to reversible scavenging generally start higher in the water column for dissolved ^{231}Pa xs (2-3 km depth) than for dissolved ^{230}Th xs (4-5 km). This is a pervasive feature in the Atlantic (Luo et al., 2010; Moran et al., 2002; Scholten et al., 2008; Scholten et al., 2001; Vogler et al., 1998) which has been largely attributed to the advection of NADW in previous work.

At stations GT-10-01, GT11-04, GT11-06, GT11-08, and GT11-10, however, the dissolved radionuclide depletions can be clearly associated with a large increase in beam attenuation related to higher particle concentration (Fig. 3A) and presumably bottom scavenging. Additionally, the near-bottom waters at GT11-16 (mid-Atlantic ridge) and GT10-09 (African margin) have a more modest increase in C_p, but very large dissolved phase depletions. The near-bottom particles at these two sites showed a clear enrichment in metal oxides (Lam et al., this issue), the former being up

to 40% authigenic Fe oxides from a hydrothermal plume at the mid-Atlantic ridge, the latter being enrichment of authigenic Fe and Mn oxides (each 2-3% of the particle mass) related to reducing conditions in the surface sediments created by organic matter diagenesis. It thus seems likely that bottom scavenging due to increased particle abundance and/or unique particulate chemistry is at least as significant as ventilation in regulating the distributions of dissolved ^{230}Th xs and ^{231}Pa xs across the North Atlantic. In section 3.3, we give a few examples of how ventilation and bottom scavenging may be convolved in determining ^{230}Th xs and ^{231}Pa xs distributions. The de-convolution of these effects requires sensitivity testing in 3-dimensional ocean models which is beyond the scope of this study.

3.2 Quantification of boundary scavenging

Enhanced removal of trace elements at ocean margins is supported by advective and diffusive fluxes that arise due to the lateral concentration gradients imposed by lateral gradients in scavenging intensity (Bacon, 1988). To quantify the magnitude of this flux, one can calculate the lateral concentration gradients from concentration profiles. Since radionuclides are exchanged between dissolved and adsorbed forms faster than they are removed to the seafloor (Bacon and Anderson, 1982), for mass continuity, one must consider the total radionuclide concentration (dissolved plus particulate). In Figure 4, we plot particulate and total ^{230}Th xs and ^{231}Pa xs for the stations between Mauritania and GT11-22. Total ^{230}Th xs concentrations (Fig. 4C) are consistently lower at stations closer to the African margin, at nearly all depths. The lateral gradient in total ^{231}Pa xs (Fig. 4D), on the other hand, is smaller than can be resolved within our analytical uncertainties. These observations are consistent with the boundary scavenging concept (Fig. 2). At the margin, ^{230}Th concentrations can be depleted with respect to ocean interior concentrations to a greater extent than ^{231}Pa concentrations. This is due to the longer ocean residence time of ^{231}Pa.

Lateral mixing and advection is not fast enough to erase the margin-interior ^{230}Th concentration gradient imposed by scavenging, whereas a lateral flux toward the margin is supported for ^{231}Pa. Consequently, both dissolved and particulate ^{231}Pa/^{230}Th xs ratios are higher at the margin versus the interior (Fig. 4E-F), as predicted by Bacon (1988).

In one dimension (x, an isopycnal surface, since circulation occurs preferentially along lines of constant seawater density), for total ^{230}Th xs (Th), the steady-state mass balance is:

$$\frac{dTh}{dt} = P - S\frac{dTh_p}{dz} - u\frac{dTh}{dx} + K_H\frac{d^2Th}{dx^2} \qquad \text{Eq. 1}$$

P is production due to ^{234}U decay. S is the particle sinking rate which, when multiplied by the vertical gradient of particulate ^{230}Th concentration (second term on right-hand side of Eq. 1), represents the downward flux by scavenging. The third and fourth terms on the right-hand side of Eq. 1 represents lateral fluxes due to advection (isopycnal velocity, u, multiplied by the first isopyncal concentration gradient) and eddy diffusion (isopycnal eddy diffusion coefficient, K_H, multiplied by the second isopycnal concentration gradient), respectively.

In order to affect the steady-state mass balance, the advective and diffusive terms must occur on a timescale appropriate to the residence time, τ, of the tracer. The residence times, as defined by the water column inventory of radionuclide divided by its integrated production in the water column, between GT10-09 and GT11-22 for ^{230}Th and ^{231}Pa, respectively, are 10-28 yrs and 120-150 yrs. The corresponding length scales over which lateral eddy diffusivity should be considered are ~800-1300 km for ^{230}Th and 2750-3080 km for ^{231}Pa ($\Delta x = \sqrt{2K_H\tau}$, parameterizing eddy diffusivity as a random walk process), using $K_H = 10^3$ m^2 s^{-1}, as determined in the Northeast Atlantic (Ledwell et al., 1998). The advective length scale ($\Delta x = u\tau$) depends linearly on the current speed and will be >1500 km for both radionuclides if u is greater than a typical deep current speed of 2 mm/s. However, because east-west velocities cyclically change direction in this region

(Zenk et al., 1991) and their magnitude is difficult to estimate for the deep ocean, we do not attempt to quantify the advective flux.

The isopycnal gradients in ^{230}Th are estimated discretely using the observations from GT10-09, GT10-10, GT10-11 and GT10-12 (Fig. 4C). We do not include GT11-22 in the analysis because it makes the transect larger than the ^{230}Th-mixing length scale (~1400 km). The isopycnal ^{231}Pa gradients are smaller than can be resolved within our analytical uncertainty. Th-230 concentrations were interpolated onto a common set of isopycnals (Fig. 5A), and because GT10-11 and GT10-12 are nearly indistinguishable we average these two profiles and consider the average profile representative of the region at the mid-point between the two stations. Uncertainties were accounted for and propagated in the calculations by assuming a conservative analytical uncertainty for total ^{230}Th xs of 1.5%. Two isopycnal gradients (Fig. 5B) were calculated by differencing the concentration profiles, between GT10-09 and GT10-10 and between GT10-10 and GT10-11/12, and dividing by the lateral distance between the stations. A positive gradient is defined as lower concentration in the east (leading to lateral fluxes toward Mauritania). Then the second isopycnal gradient (Fig. 5C) was calculated by differencing the two isopycnal gradient profiles and dividing by the distance between the mid-points of the stations used to calculate the first gradient (Fig. 5D).

The second isopycnal gradient is variable above γ_n = 27.8 (1.2 km depth), but below this density surface, in the bulk of the water column, the gradient is consistently positive (down gradient toward Mauritania). By multiplying the d^2Th/dx^2 profile by K_H (10^3 m^2 s^{-1}), and integrating with depth (~0-3 km), we estimate the lateral convergence of ^{230}Th xs to the margin (technically between two boxes, encompassing stations GT10-10/11/12 and GT10-09/10, respectively) as 509 ± 171 mBq m^{-2} yr^{-1}. In 3 km of seawater, ^{230}Th production due to U decay is

346 1237 mBq m^{-2} yr^{-1} and thus the diffusive flux adds 41 ± 14% to the water column production in
347 the margin box (and removes the equivalent from production in the open-ocean box). This is
348 consistent with the upper limit for the model-derived redistribution of water column ^{230}Th
349 (Henderson et al., 1999).

350 Th-230 normalized sediment fluxes will therefore be biased (underestimated) by up to 30-
351 50% for core sites at highly productive continental margins such as offshore Mauritania. The
352 magnitude of the complementary bias (overestimation) in ^{230}Th-normalized fluxes in the interior
353 ocean is likely to be smaller than 30-50%. This is because the ^{230}Th added to the relatively small
354 zone of high productivity at the margin is drawn from a much larger pool of the subtropical North
355 Atlantic gyre. The subtropical gyre ^{230}Th budget, however, cannot be fully constrained here
356 because there are likely additional lateral removal fluxes of ^{230}Th to other more expansive high
357 productivity regions such as the equatorial or subpolar North Atlantic (Henderson et al., 1999).

358 Interestingly, the degree of boundary scavenging (and its impact on lateral ^{230}Th
359 redistribution) may have changed since the last glacial maximum (Lao et al., 1992). Nonetheless,
360 the 40% redistribution estimate can be seen as close to a global maximum (in the modern ocean at
361 least) since the Canary Current upwelling regime in which our observations are made produces
362 one of the largest lateral gradients in productivity (and in turn particle flux) in the world
363 (Behrenfeld and Falkowski, 1997). Thus our finding supports the use of ^{230}Th-normalization to
364 reconstruct sediment fluxes within cited uncertainties (François et al., 2004).

365 Although we cannot directly estimate the magnitude of boundary scavenging for ^{231}Pa
366 because the lateral water column ^{231}Pa gradients are not discernible, we can use the ^{230}Th results
367 in conjunction with the particulate ^{231}Pa/^{230}Th xs data (Fig. 4F) to estimate the redistribution of
368 ^{231}Pa. The near-bottom ^{231}Pa/^{230}Th xs ratio of particulate material, $(Pa/Th)_{bottom}$, should represent

the ratio of sinking flux for the two elements. If both elements were being buried at their production rate by U decay, we would expect this ratio to be 0.093 (activity units, see dotted line, Fig. 4F). Therefore the ratio of sinking flux to overlying production for ^{231}Pa, $(F/P)_{Pa}$, is proportional to that of ^{230}Th, weighted by the deviation of the near-bottom particulate material from the production ratio:

$$(F/P)_{Pa} = (F/P)_{Th} * (Pa/Th)_{bottom} / 0.093 \quad \text{(Eq. 2)}$$

The average particulate ^{231}Pa/^{230}Th ratio of the two near bottom samples at GT10-09, within about 100 m of the seafloor, is 0.18 (Fig. 4F). Using $(F/P)_{Th} = 1.4$ as calculated above, we estimate that ^{231}Pa is being buried at 2.7 times its production in the overlaying water column at this site. While clearly a region of enhanced ^{231}Pa removal, this region will likely not account for observed depletion of ^{231}Pa in deep North Atlantic sediment. High productivity areas such as GT10-09, where boundary scavenging of ^{231}Pa is occurring, are likely only a small volumetric percentage of the basin (Lippold et al., 2012b). This is indicated by the sharp decrease in particulate ^{231}Pa/^{230}Th xs ratio between stations GT10-09 and GT10-10 (Fig. 4F). Nonetheless, more detailed mapping of the extent of this type of enhanced ^{231}Pa burial on the North African margin is required before its impact on the basin-wide Pa budget can be quantified (Burke et al., 2011; Marchal et al., 2000).

3.3 Bottom scavenging and ventilation: convoluted influences across the North Atlantic

Both ^{231}Pa xs and ^{230}Th xs (Fig. 3) have negative concentration anomalies associated with the high salinity waters of the Mediterranean Outflow Water (MOW, ~1 km depth at station GT10-01, Fig. 1). This is expected due to the high particle load of MOW, a result of the interaction of the flow of Mediterranean Water over the Gibralter Strait and the Iberian margin (McCave and Hall, 2002; Thorpe, 1972), which is known to enhance scavenging of ^{234}Th and ^{228}Th (half-life 1.8

yrs, parent ^{228}Ra) (Schmidt, 2006). Unexpectedly, the low radionuclide concentrations (causing negative deviations to a linear profile) appear to be advected along with the flow of MOW to station GT10-03 and even to GT10-05 for ^{231}Pa xs, while the high particle concentrations (on the basis of C_p, Fig. 3A) are not, i.e. the downstream effects are not necessarily due to in-situ scavenging. There is a strong boundary in ^{231}Pa xs concentrations and water mass age between GT10-05 and GT10-07 at 2 km depth (Fig. 3), indicating more recently ventilated water to the north, making it difficult to separate the downstream effects of specifically MOW from a large-scale influence of other NADW components. This is the first of several examples of how ventilation and bottom scavenging combine to produce low concentration anomalies in the water column radionuclide distributions.

Second, we look in more detail (Fig. 6) at the impact of the enhanced scavenging observed at station GT11-16, also known as the TAG hydrothermal site (Rona, 1980; Rona et al., 1984). Clearly, dissolved ^{230}Th xs and ^{231}Pa xs are removed from solution in the observed hydrothermal plume around 3.3 km depth (Figs. 3B, 3D, 6). But it also appears that the low concentration anomaly in the plume is dispersed by circulation to shallower depths in the water column. The TAG concentration profile departs negatively for dissolved ^{230}Th xs at 2.1 km, and for dissolved ^{231}Pa xs at 1.5 km. Furthermore, the low radionuclide concentrations appear to be advected to sites west of the ridge. For both radionuclides at 2.5 km depth, concentrations at GT11-14 are lower than they are to the west at GT11-12, opposite to the expected trend due to water mass ageing.

Westward and shoaling propagation of the hydrothermal scavenging anomaly is consistent with theory, i.e. buoyant plume water rising and heading west due to geostrophic considerations (Speer, 1989). We note that this type of hydrothermal circulation will not be accounted for in the mean age estimates. This type of "downstream" hydrothermal effects (both vertical and lateral,

Fig. 6) are not caused only by the observed venting at the TAG site but are more likely the integrated result of vent sites all along the ridge (German et al., 2010). This result is support for the hypothesis that hydrothermal vents are a basin-scale sink of Pa in the deep ocean (Hayes et al., 2013). However, because the observed hydrothermal anomaly and its far-field effect occur in a region with strong zonal and meridional gradients in water mass age, it is difficult to remove the influence of ventilation and isolate the hydrothermal scavenging magnitude. For instance, one could estimate the removal flux of ^{231}Pa (or ^{230}Th) by using the deficit of the observed concentration profile compared to a linear profile (expected due to reversible scavenging) (Deng et al., 2014). The expected profile however cannot be chosen *a priori*, because in a region of recent deep water ventilation one does not expect a linear profile.

Similarly, along Line W (GT11-01 thru GT11-10), dissolved ^{230}Th xs and ^{231}Pa xs concentrations are clearly depleted near the bottom (Fig. 3B, D) due to increased particle concentrations in nepheloid layers (Fig. 3A). Depletion of ^{230}Th and ^{231}Pa below 3.5 km depth cannot be attributed to ventilation, the conventional explanation (e.g., Luo et al., 2010), because ventilation time scales increase with depth below 3.5 km (Fig. 3E). Nonetheless, the fact that ^{230}Th and ^{231}Pa concentrations at mid-depth (1-3km) along Line W, the depth range of maximum southward NADW transport (Cunningham et al., 2007; Kanzow et al., 2010; Talley et al., 2003), are much lower than at the corresponding depths in the eastern basin at GT11-20 and GT11-22 (Fig. 3B, D), where particle concentrations (C_p values) are similar to those along Line W (Fig. 3A), seems clearly related to the east-west gradient in mean age. Radionuclide depletions due to bottom scavenging and recent ventilation again here seem convolved in a way that is difficult to untangle with static tracer observations.

In yet another combination of influences, dissolved ^{230}Th xs and ^{231}Pa xs concentrations both decrease toward the bottom at GT11-20 and GT11-22 at ~4 km and 2.5 km depth, respectively, where there is no evidence for increased particle concentrations or recent ventilation. While the deep water in the Northeast Atlantic has been long isolated from the atmosphere (>500 yrs), it may not have been this long since a significant scavenging event occurred. The inflow of NEADW from the Vema and Romanche Fracture Zones occurs on a timescale of 30 years based on radiocarbon distributions (Schlitzer et al., 1985). The mid-Atlantic ridge is associated with enhanced turbulent mixing because of its complex topography (Polzin et al., 1996) and with metalliferous sediments from hydrothermal activity. Both of these factors could cause bottom scavenging of ^{230}Th and ^{231}Pa from water flowing through the gaps in the ridge, the former via resuspension of sediments and the latter by the increased scavenging efficiency of Fe-Mn oxides. A radionuclide depleted signal could then be advected northward, carrying with it its scavenging history. While this scenario is highly speculative, such are the possible interactions between deep water flow and bottom scavenging that need to be accounted for in a fuller understanding of the marine cycling of ^{230}Th and ^{231}Pa.

3.4 Apparent controls on seawater and sedimentary ^{231}Pa/^{230}Th ratios

Sensitivity tests in a scavenging-circulation ocean model, which can vary bottom scavenging intensity and ventilation timescales independently, may be able to resolve the significance of each process in determining radionuclide distributions in the North Atlantic. This uncertainty notwithstanding, it is informative to inspect the section of the dissolved ^{231}Pa/^{230}Th xs ratio (Fig. 3C) with a motivation to examine its proxy applications. High ratios along the Cape Verde transect are consistent with boundary scavenging as discussed in section 3.2. In the areas of clear bottom scavenging along Line W and at the TAG hydrothermal site, the ratio is also elevated

460 above the corresponding mid-depth values. This is because the ^{230}Th is scavenged more intensely
461 (larger depletion from the dissolved phase) relative to ^{231}Pa at these locations. In analogy to the
462 boundary scavenging due to lateral gradients in scavenging intensity, the bottom scavenging sites
463 may also act as preferential sinks for Pa. Because of its longer residence time, dispersive fluxes of
464 Pa into the bottom scavenging sites likely result in a greater Pa burial rate than would occur in the
465 absence of bottom scavenging (Deng et al., 2014).

466 The impact of ventilation on the dissolved ^{231}Pa/^{230}Th xs distribution (Fig. 3C), however,
467 is not obvious. For instance, between 2-3 km depth (excluding GT11-16) the ^{231}Pa/^{230}Th ratio
468 changes very little between 500 and 4200 km section distance (Fig. 3C), along which the mean
469 age has a strong lateral gradient between roughly 80 yrs in the west and 400 yrs in the east. This
470 range in age is the exact time period in which one expects the strongest return to a steady-state of
471 ^{231}Pa concentrations after ventilation (Gherardi et al., 2010), according to a 1-dimensional mixing-
472 scavenging model (Moran et al., 2001; Rutgers v. d. Loeff and Berger, 1993). The dissolved
473 ^{231}Pa/^{230}Th xs ratio of course increases further toward the African margin as ventilation age also
474 increases, but this is primarily due to the stronger removal of dissolved ^{230}Th xs (boundary
475 scavenging, sec. 3.2) at the eastern margin.

476 The observed zonal gradient in dissolved ^{231}Pa/^{230}Th xs (Fig. 3C) is not consistent with
477 removal of ^{231}Pa by southward flow between 2-3 km depth, which one expects to be strongest in
478 the west (Wunsch and Heimbach, 2006, 2013). That said, we cannot refute that the large-scale
479 deficit of ^{231}Pa in North Atlantic sediments (Lippold et al., 2012a; Yu et al., 1996) is consistent
480 with some amount of zonally-integrated southward ^{231}Pa transport from the North Atlantic to the
481 South Atlantic. This interpretation is supported by our particulate ^{231}Pa/^{230}Th xs data being mostly
482 below the production ratio (Fig. 4F) and by transport analysis of recent water column data from

483 the South Atlantic (Deng et al., 2014). Whether the $^{231}Pa/^{230}Th$ distribution (as opposed to ^{231}Pa
484 itself) is also responding to a zonally integrated southward flow of NADW remains to be
485 demonstrated in a 3-D dimensional circulation-scavenging model.

486 For instance, in the deep basins (4-6 km depth), likely not influenced by the African margin
487 processes, the dissolved $^{231}Pa/^{230}Th$ xs ratio is higher on the eastern side of the mid-Atlantic ridge,
488 as expected from the trend in mean age (Fig. 3D), perhaps reflecting the integrated removal of
489 ^{231}Pa (relative to ^{230}Th) by southward flow throughout the water column. Additionally, the ratio
490 decreases with depth (below 1 km and away from bottom scavenging sites), most significantly at
491 the deep central basin stations GT11-12 and GT11-20. The decrease with depth of the $^{231}Pa/^{230}Th$
492 ratio in the Atlantic has been suggested to reflect the southward export of ^{231}Pa by deep water
493 circulation (Lippold et al., 2011; Luo et al., 2010) based on 2-dimensional ocean models which
494 average out the east-west gradient in ventilation observed in our transect (Fig. 3E), also suggesting
495 a zonally-integrated effect of ventilation.

496 The influence of circulation may interestingly be more significant in the upper 1-1.2 km.
497 High $^{231}Pa/^{230}Th$ xs ratios near the surface are consistent with ^{230}Th being more intensely
498 scavenged out of the mixed layer, but a secondary subsurface maximum in dissolved $^{231}Pa/^{230}Th$
499 xs ratio around 1 km depth is observed at nearly every station. In the section between the mid-
500 ocean ridge and Mauritania, the secondary dissolved $^{231}Pa/^{230}Th$ xs maximum overlaps with AAIW
501 (cf. Fig. 1). The persistence of the $^{231}Pa/^{230}Th$ maximum in the more northern parts of the transect,
502 however, does not support an association with AAIW. An alternative scenario is that a high
503 $^{231}Pa/^{230}Th$ ratios throughout shallow water (0-1200 m), related to more intense scavenging of
504 ^{230}Th, is overprinted with the strong minimum around 500 m depth which could be related to the
505 low ^{231}Pa content and rapid ventilation of EDW. Yet another possible scenario is that the

subsurface dissolved $^{231}Pa/^{230}Th$ xs maximum is related to the preferential regeneration of dissolved ^{231}Pa released during diatom dissolution (since biogenic opal is a strong scavenger of ^{231}Pa (Chase et al., 2002)). This is not supported, however, by either the silicic acid distribution (except within AAIW, Fig. 7B) or the particulate opal distribution (Lam et al., submitted). In any case, the possibility of ^{231}Pa (and perhaps $^{231}Pa/^{230}Th$) tracing shallow or intermediate water circulation is worth further attention since its longer-lived removal timescale and uniform production offers a complement to the traditional transient tracers of shallow circulation (^{3}H-^{3}He, CFC's).

As a way of summarizing these observations we cross-plot the dissolved $^{231}Pa/^{230}Th$ xs data with another potential circulation tracer measured on the same water samples, silicic acid. The silicic acid distribution along our transect (Fig. 7B) has a resemblance to the inverse estimates of mean age (Fig. 3E). Silicic acid is added to deep water through the dissolution of diatom opal exported from surface water and accumulates with deep water age (Broecker and Peng, 1982). Furthermore, its distribution is sensitive to the overturning circulation since NADW has very low (preformed) silicic acid and southern-sourced waters (AABW and AAIW) have much higher end-member concentrations (Sarmiento et al., 2007). There is a wide scatter in the relationship between dissolved $^{231}Pa/^{230}Th$ xs and silicic acid (Fig. 7A) and the overall negative trend reflects that fact the $^{231}Pa/^{230}Th$ ratio generally decreases with depth while silicic acid (and mean age) increase with depth. At some given depths (color scheme of points in Fig. 7A), however, $^{231}Pa/^{230}Th$ may be positively related with silicic acid. For instance, around 1 km depth (dark blue points in Fig. 7A) a positive trend possibly related to the influence of AAIW can be seen. Some of the high $^{231}Pa/^{230}Th$ values at 3-4 km depth, however, are related to locations of bottom scavenging (marked in Fig. 7A) and therefore cannot be ascribed to water mass ageing.

While a basin-sale, integrated influence of the southward export of NADW cannot be ruled out, the distribution of dissolved $^{231}Pa/^{230}Th$ appears to be insensitive to water mass age across the North Atlantic. In order to validate the use of the $^{231}Pa/^{230}Th$ ratio as a quantitative paleo-indicator of the AMOC, a more complex conceptual model needs to be developed, including the influences of boundary scavenging and bottom scavenging demonstrated here.

4. Summary

The cycling of ^{230}Th and ^{231}Pa in the ocean is complex. Deviations from the behavior expected from a simple model of reversible scavenging are apparent across the North Atlantic and improved spatial resolution allows us to study them in greater detail than has been done before. Boundary scavenging of ^{230}Th in an exceptionally productive region off Northwest Africa can be constrained to 40 ± 10 % of its water column production, helping to quantify the uncertainties associated with ^{230}Th-normalized sediment fluxes. Enhanced removal of ^{231}Pa occurs on the Africa margin as well but quantitative conclusions about the significance of this sink in the basin-scale Pa budget cannot be made without more detailed mapping of the region. Both recent ventilation and bottom scavenging cause deep-water depletions of ^{230}Th and ^{231}Pa. The dissolved $^{231}Pa/^{230}Th$ ratio traces locations of intense scavenging intensity while its distribution in the transect is not consistent with a simple relationship to water-mass age. We observe several examples where the effects of scavenging and ventilation are convolved which provide excellent test cases for sensitivity studies of removal mechanisms in future ocean modeling of these isotopes. Circulation and scavenging affect many trace metals of biogeochemical and paleoceanographic interest (e.g. Fe, Co, Al), and thus further constraining the cycling of ^{230}Th and ^{231}Pa will be of broad appeal in the oceanographic community.

Acknowledgements

Funding for ship time, sampling operations, and hydrographic data was provided by the U. S. National Science Foundation to the US GEOTRACES North Atlantic Transect Management team of W. Jenkins (OCE-0926423), E. Boyle (OCE-0926204), and G. Cutter (OCE-0926092). Radionuclide studies were supported by NSF (OCE-0927064 to L-DEO, OCE-0926860 to WHOI, OCE-0927757 to URI, and OCE-0927754 to UMN). LFR was also supported by Marie Curie Reintegration Grant and the European Research Council. The crew of the R/V *Knorr*, the Ocean Data Facility team (Mary Johnson, Rob Palomares, Susan Becker, Melissa Miller and Courtney Schatzman), and the science team samplers for Niskin bottles and in situ pumps (Katharina Pahnke, Brett Longworth, Paul Morris, Daniel Ohnemus, Kuanbo Zhou, Sylvain Rigaud and Stephanie Owens) are all acknowledged for their critical roles in the success of these cruises. On-shore analysis efforts of Maureen Auro, Joanne Boudreau, and the WHOI Plasma Facility are greatly appreciated. Figures 1, 3 and 7 were created using Ocean Data View (Schlitzer, 2011). We thank Alex Thomas and an anonymous reviewer for improving the quality of the manuscript.

Figure Captions

Figure 1 Map of GEOTRACES section GA03, the U.S. GEOTRACES North Atlantic Transect and section of salinity as measured in the Niskin bottle rosette casts. Neutral density overlays define, in order of increasing density, the bottom of Eighteen Degree Water (EDW), Upper and Classic Labrador Sea Water (ULSW/CLSW), Iceland-Scotland Overflow Water (ISOW), Denmark-Strait Overflow Water (DSOW) and Antarctic Bottom Water (AABW), defined largely for the western basin by Toole et al. (2010) and LeBel et al. (2008). The deep (>3 km) eastern basin is filled with a more homogeneous water mass named Northeast Atlantic Deep Water (NEADW) (Schlitzer et al., 1985). The southeastern section is influenced by Antarctic Intermediate Water (AAIW) at about ~1 km depth and the northeastern margin is clearly influenced by the high salinity Mediterranean Outflow Water (MOW). Presented in this paper is dissolved radionuclide data for all stations listed here, and a sub-set of particulate radionuclide data for stations marked with a black diamond.

Figure 2. Schematic representation of boundary scavenging. Along distance from an ocean margin, particle flux (in arbitrary units, a.u.) increases nearly exponentially. The particulate and dissolved $^{231}Pa/^{230}Th$ ratio are expected to increase with increasing particle flux, associated with increasing scavenging intensity. Note that the particulate $^{231}Pa/^{230}Th$ ratios overlap the production activity ratio (A.R., 0.093) produced from uranium decay, whereas the dissolved ratios are roughly 10 times higher due to the preferential scavenging of ^{230}Th from seawater. The longer residence time of ^{231}Pa, compared to that of ^{230}Th, allows a greater lateral flux of ^{231}Pa down the concentration gradient toward the margin. This results in increased sinking vertical flux of ^{231}Pa at the margin, at the expense of a lower vertical flux in the ocean interior. In contrast, the sinking ^{230}Th flux is relatively uniform since its lateral movement is more limited. Therefore the water column sustains greater lateral concentration gradients in ^{230}Th than in ^{231}Pa. The numerical values used here are simply for illustration and do not represent actual observations.

Figure 3 Property sections of the US GEOTRACES North Atlantic transect. (A) Particle beam attenuation coefficient, Cp, determined by transmissometer. CTD casts are marked in black. (B) Dissolved (<0.45 μm) ^{230}Th, (C) $^{231}Pa/^{230}Th$ activity ratio, and (D) ^{231}Pa. Black dots indicate

discrete measurements. (E) Mean age of seawater since being at the surface as estimated by Khatiwala et al. (2012). Station locations for radioncuclide data are as labeled in the map of Figure 1. Panels A and E, in addition, have data from shallow "demi" stations occupied in between full depth stations, as plotted in the inset map of panel E. See Fig. 1 for neutral density surfaces not included here for clarity.

Figure 4 Depth profiles of particulate (0.45-51 μm) (A, B) and total (C, D) ^{230}Th xs and ^{231}Pa xs and the dissolved (<0.45 μm) (E) and particulate (F) ^{231}Pa/^{230}Th xs ratio from stations along a zonal transect between Mauritania and west of Cape Verde. The dashed lines in (E) and (F) represent the activity ratio of ^{231}Pa/^{230}Th produced by uranium decay (0.093). Legend relates station names as located in Figure 1.

Figure 5 (A) Depth profiles of total ^{230}Th interpolated onto a common set of isopycnal surfaces. (B) Discretely calculated lateral concentration gradients in total ^{230}Th. Units are μBq x 10^{-3} per kilogram seawater per kilometer distance (C) Discretely calculated second lateral concentration gradient in total ^{230}Th. Units are μBq x 10^{-6} per kilogram seawater per square kilometer (D) Schematic demonstrating the concept of calculating lateral gradients using the concentration difference between depth profiles and the distance separating the profile locations along the Cape Verde transect.

Figure 6 Depth profiles of dissolved ^{230}Th and ^{231}Pa from the hydrothermal TAG site, GT11-16, and the surrounding stations. As inferred from the section (Fig. 3), it is possible that the strong removal of both isotopes at hydrothermal plumes along the Mid-Atlantic Ridge causes downstream radionuclide depletion, with respect to the linear increase in concentration with depth expected from reversible scavenging, at sites to the west of the ridge (GT11-14 and GT11-12) but not significantly to the east (GT11-18).

Figure 7 (A) Dissolved ^{231}Pa/^{230}Th xs ratios versus silicic acid measured in the same samples. The arrow indicates a possible positive trend between ^{231}Pa/^{230}Th xs ratios and silicic acid carried by Antarctic Intermediate Water (AAIW). The circled points represent locations of bottom scavenging which causes elevated ^{231}Pa/^{230}Th xs ratios and are unrelated to the circulation patterns traced by silicic acid. (B) Silicic acid distribution along the North Atlantic transect.

References

Andersen, M.B., Stirling, C.H., Zimmermann, B., Halliday, A.N., 2010. Precise determination of the open ocean ^{234}U/^{238}U composition. Geochem. Geophys. Geosyst. 11, Q12003.

Anderson, R.F., 1982. Concentration, vertical flux, and remineralization of particulate uranium in seawater. Geochim. Cosmochim. Acta 46, 1293-1299.

Anderson, R.F., Bacon, M.P., Brewer, P.G., 1983. Removal of ^{230}Th and ^{231}Pa at ocean margins. Earth Planet. Sci. Lett. 66, 73-90.

637 Anderson, R.F., Fleisher, M.Q., Biscaye, P.E., Kumar, N., Dittrich, B., Kubik, P., Suter, M., 1994.
638 Anomalous boundary scavenging in the Middle Atlantic Bight: evidence from ^{230}Th, ^{231}Pa, ^{10}Be and ^{210}Pb.
639 Deep Sea Res. Pt. II 41, 537-561.

640 Anderson, R.F., Fleisher, M.Q., Robinson, L.F., Edwards, R.L., Hoff, J., Moran, S.B., Rutgers van der
641 Loeff, M.M., Thomas, A.L., Roy-Barman, M., François, R., 2012. GEOTRACES intercalibration of
642 ^{230}Th, ^{232}Th, ^{231}Pa, and prospects for ^{10}Be. Limnol. Oceanogr. Methods 10, 179-213.

643 Anderson, R.F., Lao, Y., Broecker, W.S., Trumbore, S.E., Hofmann, H.J., Wolfli, W., 1990. Boundary
644 scavenging in the Pacific Ocean: a comparison of ^{10}Be and ^{231}Pa. Earth Planet. Sci. Lett. 96, 287-304.

645 Auro, M.E., Robinson, L.F., Burke, A., Bradtmiller, L.I., Fleisher, M.Q., Anderson, R.F., 2012.
646 Improvements to 232-thorium, 230-thorium, and 231-protactinium analysis in seawater arising from
647 GEOTRACES intercalibration. Limnol. Oceanogr.: Methods 10, 464-474.

648 Bacon, M.P., 1984. Glacial to interglacial changes in carbonate and clay sedimentation in the Atlantic
649 Ocean estimated from ^{230}Th measurements. Chem. Geol. 46, 97-111.

650 Bacon, M.P., 1988. Tracers of chemical scavenging in the ocean: boundary effects and large-scale
651 chemical fractionation. Philos. Trans. R. Soc. London, Ser. A 325, 147-160.

652 Bacon, M.P., Anderson, R.F., 1982. Distribution of thorium isotopes between dissolved and particulate
653 forms in the deep sea. J. Geophys. Res. 87, 2045-2056.

654 Bacon, M.P., Rutgers v. d. Loeff, M.M., 1989. Removal of thorium-234 by scavenging in the bottom
655 nepheloid layer of the ocean. Earth Planet. Sci. Lett. 92, 157-164.

656 Bacon, M.P., Spencer, D.W., Brewer, P.G., 1976. ^{210}Pb/^{226}Ra and ^{210}Po/^{210}Pb disequilibria in seawater and
657 suspended particulate matter. Earth Planet. Sci. Lett. 32, 277-296.

658 Baker, E.T., Lavelle, J.W., 1984. The effect of particle size on the light attenuation coefficient of natural
659 suspensions. J. Geophys. Res.: Oceans 89, 8197-8203.

660 Behrenfeld, M.J., Falkowski, P.G., 1997. Photosynthetic rates derived from satellite-based chlorophyll
661 concentration. Limnol. Oceanogr. 42, 1-20.

662 Biscaye, P.E., Eittreim, S.L., 1977. Suspended particulate loads and transports in the nepheloid layer of
663 the abyssal Atlantic Ocean. Mar. Geol. 23, 155-172.

664 Bishop, J.K., Lam, P.J., Wood, T.J., 2012. Getting good particles: Accurate sampling of particles by large
665 volume in-situ filtration. Limnol. Oceanogr.: Methods 10, 681-710.

666 Bishop, J.K.B., 1986. The correction and suspended particulate matter calibration of Sea Tech
667 transmissometer data. Deep Sea Res. Pt. A 33, 121-134.

668 Brewer, P.G., Spencer, D.W., Biscaye, P.E., Hanley, A., Sachs, P.L., Smith, C.L., Kadar, S., Fredericks,
669 J., 1976. The distribution of particulate matter in the Atlantic Ocean. Earth Planet. Sci. Lett. 32, 393-402.

670 Broecker, W., 2008. Excess sediment ^{230}Th: Transport along the sea floor or enhanced water column
671 scavenging? Global Biogeochem. Cycles 22, GB1006.

672 Broecker, W.S., Blanton, S., Smethie, W.M., Ostlund, G., 1991. Radiocarbon decay and oxygen
673 utilization in the Deep Atlantic Ocean. Global Biogeochem.Cycles 5, 87-117.

674 Broecker, W.S., Peng, T.-H., 1982. Tracers in the Sea. Lamont-Doherty Geol. Obs., Palisades, NY.

675 Broecker, W.S., Takahashi, T., Stuiver, M., 1980. Hydrography of the central Atlantic—II waters beneath
676 the Two-Degree Discontinuity. Deep Sea Res. Pt. A 27, 397-419.

677 Bruland, K., Lohan, M., 2003. Controls of Trace Metals in Seawater. Treatise on Geochemistry 6, 23-47.

678 Burke, A., Marchal, O., Bradtmiller, L.I., McManus, J.F., François, R., 2011. Application of an inverse
679 method to interpret ^{231}Pa/^{230}Th observations from marine sediments. Paleoceanography 26, PA1212.

680 Chase, Z., Anderson, R.F., Fleisher, M.Q., Kubik, P.W., 2002. The influence of particle composition and
681 particle flux on scavenging of Th, Pa and Be in the ocean. Earth Planet. Sci. Lett. 204, 215-229.

682 Cheng, H., Edwards, R.L., Hoff, J., Gallup, C.D., Richards, D.A., Asmerom, Y., 2000. The half-lives of
683 uranium-234 and thorium-230. Chem. Geol. 169, 17-33.

684 Cunningham, S.A., Kanzow, T., Rayner, D., Baringer, M.O., Johns, W.E., Marotzke, J., Longworth, H.R.,
685 Grant, E.M., Hirschi, J.J.-M., Beal, L.M., Meinen, C.S., Bryden, H.L., 2007. Temporal Variability of the
686 Atlantic Meridional Overturning Circulation at 26.5°N. Science 317, 935-938.

687 Delanghe, D., Bard, E., Hamelin, B., 2002. New TIMS constraints on the uranium-238 and uranium-234
688 in seawaters from the main ocean basins and the Mediterranean Sea. Mar. Chem. 80, 79-93.

689 DeMaster, D.J., Brewster, D.C., McKee, B.A., Nittrouer, C.A., 1991. Rates of particle scavenging,
690 sediment reworking, and longitudinal ripple formation at the HEBBLE site based on measurements of
691 ^{234}Th and ^{210}Pb. Mar. Geol. 99, 423-444.

692 Deng, F., Thomas, A.L., Rijkenberg, M.J.A., Henderson, G.M., 2014. Controls on seawater ^{231}Pa, ^{230}Th
693 and ^{232}Th concentrations along the flow paths of deep waters in the Southwest Atlantic. Earth Planet. Sci.
694 Lett. 390, 93-102.

695 François, R., Bacon, M.P., Suman, D.O., 1990. Thorium-230 profiling in deep-sea sediments: High-
696 resolution records of flux and dissolution of carbonate in the equatorial Atlantic during the last 24,000
697 years. Paleoceanography 5, 761-787.

François, R., Frank, M., Rutgers van der Loeff, M., Bacon, M.P., Geibert, W., Kienast, S., Anderson, R.F., Bradtmiller, L., Chase, Z., Henderson, G., 2007. Comment on" Do geochemical estimates of sediment focusing pass the sediment test in the equatorial Pacific?" by M. Lyle et al. Paleoceanography 22.

François, R., Frank, M., Rutgers van der Loeff, M.M., Bacon, M.P., 2004. ^{230}Th normalization: An essential tool for interpreting sedimentary fluxes during the late Quaternary. Paleoceanography 19, PA1018.

Gardner, W.D., Biscaye, P.E., Zaneveld, J.R.V., Richardson, M.J., 1985. Calibration and comparison of the LDGO nephelometer and the OSU transmissometer on the Nova Scotian rise. Mar. Geol. 66, 323-344.

German, C.R., Fleer, A.P., Bacon, M.P., Edmond, J.M., 1991. Hydrothermal scavenging at the Mid-Atlantic Ridge: radionuclide distributions. Earth Planet. Sci. Lett. 105, 170-181.

German, C.R., Higgs, N.C., Thomson, J., Mills, R., Elderfield, H., Blusztajn, J., Fleer, A.P., Bacon, M.P., 1993. A geochemical study of metalliferous sediment from the TAG Hydrothermal Mound, 26°08′N, Mid-Atlantic Ridge. J. Geophys. Res.: Solid Earth 98, 9683-9692.

German, C.R., Thurnherr, A.M., Knoery, J., Charlou, J.L., Jean-Baptiste, P., Edmonds, H.N., 2010. Heat, volume and chemical fluxes from submarine venting: A synthesis of results from the Rainbow hydrothermal field, 36°N MAR. Deep Sea Res. Pt. I 57, 518-527.

Gherardi, J.M., Luo, Y., Francois, R., McManus, J.F., Allen, S.E., Labeyrie, L., 2010. Reply to comment by S. Peacock on "Glacial-interglacial circulation changes inferred from ^{231}Pa/^{230}Th sedimentary record in the North Atlantic region". Paleoceanography 25, PA2207.

Hayes, C.T., Anderson, R.F., Jaccard, S.L., François, R., Fleisher, M.Q., Soon, M., Gersonde, R., 2013. A new perspective on boundary scavenging in the North Pacific Ocean. Earth Planet. Sci. Lett. 369-370, 86-97.

Henderson, G.M., Anderson, R.F., 2003. The U-series Toolbox for Paleoceanography. Rev. Mineral. Geochem. 52, 493-531.

Henderson, G.M., Heinze, C., Anderson, R.F., Winguth, A.M.E., 1999. Global distribution of the ^{230}Th flux to ocean sediments constrained by GCM modelling. Deep Sea Res. Pt. I 46, 1861-1893.

Jenkins, W.J., 1988. The Use of Anthropogenic Tritium and Helium-3 to Study Subtropical Gyre Ventilation and Circulation. Phil. Trans. R. Soc. London, Ser. A 325, 43-61.

Kanzow, T., Cunningham, S.A., Johns, W.E., Hirschi, J.J.M., Marotzke, J., Baringer, M.O., Meinen, C.S., Chidichimo, M.P., Atkinson, C., Beal, L.M., Bryden, H.L., Collins, J., 2010. Seasonal Variability of the Atlantic Meridional Overturning Circulation at 26.5°N. J. Clim. 23, 5678-5698.

730 Khatiwala, S., Primeau, F., Holzer, M., 2012. Ventilation of the deep ocean constrained with tracer
731 observations and implications for radiocarbon estimates of ideal mean age. Earth Planet. Sci. Lett. 325–
732 326, 116-125.

733 Krishnaswami, S., Lal, D., Somayajulu, B.L.K., Weiss, R.F., Craig, H., 1976. Large-volume in-situ
734 filtration of deep Pacific waters: Mineralogical and radioisotope studies. Earth Planet. Sci. Lett. 32, 420-
735 429.

736 Lam, P.J., Morris, P.J., 2013. In situ marine sample collection system and methods, US Non Provisional
737 Patent Application No. 13/864,655. Patent Pending, submitted April 17, 2013.

738 Lam, P.J., Ohnemus, D.C., Auro, M.E., submitted. Size fractionated major particle composition and mass
739 from the US GEOTRACES North Atlantic Zonal Transect. Deep Sea Res, Pt. II.

740 Lao, Y., Anderson, R.F., Broecker, W.S., 1992. Boundary scavenging and deep-sea sediment dating:
741 constraints from excess ^{230}Th and ^{231}Pa. Paleoceanography 7, 783-798.

742 LeBel, D.A., Smethie Jr, W.M., Rhein, M., Kieke, D., Fine, R.A., Bullister, J.L., Min, D.-H., Roether, W.,
743 Weiss, R.F., Andrié, C., Smythe-Wright, D., Peter Jones, E., 2008. The formation rate of North Atlantic
744 Deep Water and Eighteen Degree Water calculated from CFC-11 inventories observed during WOCE.
745 Deep Sea Res. Pt. I 55, 891-910.

746 Ledwell, J.R., Watson, A.J., Law, C.S., 1998. Mixing of a tracer in the pycnocline. J. Geophys. Res.:
747 Oceans 103, 21499-21529.

748 Legeleux, F., Reyss, J.-L., Floris, S., 1995. Entrainement des metaux vers les sediments sur les marges
749 continentales de l'Atlantic Est. C. R. Acad. Sci. Paris 320 (serie IIa), 1195-1202.

750 Lippold, J., Gherardi, J.-M., Luo, Y., 2011. Testing the ^{231}Pa/^{230}Th paleocirculation proxy: A data versus
751 2D model comparison. Geophys. Res. Lett. 38, L20603.

752 Lippold, J., Luo, Y., Francois, R., Allen, S.E., Gherardi, J., Pichat, S., Hickey, B., Schulz, H., 2012a.
753 Strength and geometry of the glacial Atlantic Meridional Overturning Circulation. Nature Geosci. 5, 813-
754 816.

755 Lippold, J., Mulitza, S., Mollenhauer, G., Weyer, S., Heslop, D., Christl, M., 2012b. Boundary
756 scavenging at the East Atlantic margin does not negate use of ^{231}Pa/^{230}Th to trace Atlantic overturning.
757 Earth Planet. Sci. Lett. 333–334, 317-331.

758 Luo, Y., Francois, R., Allen, S.E., 2010. Sediment ^{231}Pa/^{230}Th as a recorder of the rate of the Atlantic
759 meridional overturning circulation: insights from a 2-D model. Ocean Sciences 6, 381-400.

760 Lyle, M., Mitchell, N., Pisias, N., Mix, A., Martinez, J.I., Paytan, A., 2005. Do geochemical estimates of
761 sediment focusing pass the sediment test in the equatorial Pacific? Paleoceanography 20, PA1005.

762 Lyle, M., Pisias, N., Paytan, A., Martinez, J.I., Mix, A., 2007. Reply to comment by R. Francois et al. on
763 "Do geochemical estimates of sediment focusing pass the sediment test in the equatorial Pacific?":
764 Further explorations of ^{230}Th normalization. Paleoceanography 22, PA1217.

765 Mangini, A., Diester-Haas, L., 1983. Excesss Th-230 in sediments off NW Africa traces upwelling in the
766 past, in: Thiede, J., Suess, E. (Eds.), Coastal upwelling: Its Sediment Record (Part A). Plenum Press, New
767 York, pp. 455-470.

768 Marchal, O., François, R., Stocker, T.F., Joos, F., 2000. Ocean thermohaline circulation and sedimentary
769 ^{231}Pa/^{230}Th ratio. Paleoceanography 15, 625-641.

770 McCartney, M.S., Bennett, S.L., Woodgate-Jones, M.E., 1991. Eastward Flow through the Mid-Atlantic
771 Ridge at 11°N and Its Influence on the Abyss of the Eastern Basin. J. Phys. Oceanogr. 21, 1089-1121.

772 McCave, I.N., 1986. Local and global aspects of the bottom nepheloid layers in the world ocean. Neth. J.
773 Sea Res. 20, 167-181.

774 McCave, I.N., Hall, I.R., 2002. Turbidity of waters over the Northwest Iberian continental margin. Prog.
775 Oceanogr. 52, 299-313.

776 McManus, J.F., Francois, R., Gherardi, J.M., Keigwin, L.D., Brown-Leger, S., 2004. Collapse and rapid
777 resumption of Atlantic meridional circulation linked to deglacial climate changes. Nature 428, 834-837.

778 Moran, S.B., Charette, M.A., Hoff, J.A., Edwards, R.L., Landing, W.M., 1997. Distribution of ^{230}Th in
779 the Labrador Sea and its relation to ventilation. Earth Planet. Sci. Lett. 150, 151-160.

780 Moran, S.B., Hoff, J.A., Buesseler, K.O., Edwards, R.L., 1995. High precision ^{230}Th and ^{232}Th in the
781 Norwegian Sea and Denmark by thermal ionization mass spectrometry. Geophys. Res. Lett. 22, 2589-
782 2592.

783 Moran, S.B., Shen, C., C, Weinstein, S.E., Hettinger, L.H., Hoff, J.H., Edmonds, H.N., Edwards, R.L.,
784 2001. Constraints on deep water age and particle flux in the equatorial and South Atlantic Ocean based on
785 seawater ^{231}Pa and ^{230}Th data. Geophys. Res. Lett. 28, 3437-3440.

786 Moran, S.B., Shen, C.C., Edmonds, H.N., Weinstein, S.E., Smith, J.N., Edwards, R.L., 2002. Dissolved
787 and particulate ^{231}Pa and ^{230}Th in the Atlantic Ocean: constraints on intermediate/deep water age,
788 boundary scavenging, and ^{231}Pa/^{230}Th fractionation. Earth Planet. Sci. Lett. 203, 999-1014.

789 Nozaki, Y., Horibe, Y., Tsubota, H., 1981. The water column distributions of thorium isotopes in the
790 western North Pacific. Earth Planet. Sci. Lett. 54, 203-216.

791 Nozaki, Y., Nakanishi, T., 1985. ^{231}Pa and ^{230}Th profiles in the open ocean water column. Deep-Sea Res.
792 Pt. A 32, 1209-1220.

793 Okubo, A., Obata, H., Gamo, T., Yamada, M., 2012. ^{230}Th and ^{232}Th distributions in mid-latitudes of the
794 North Pacific Ocean: Effect of bottom scavenging. Earth Planet. Sci. Lett. 339–340, 139-150.

795 Polzin, K.L., Speer, K.G., Toole, J.M., Schmitt, R.W., 1996. Intense mixing of Antarctic Bottom Water in
796 the equatorial Atlantic Ocean. Nature 380, 54-57.

797 Richardson, M.J., 1987. Particle size, light scattering and composition of suspended particulate matter in
798 the North Atlantic. Deep Sea Res. Pt. A 34, 1301-1329.

799 Robert, J., Miranda, C.F., Muxart, R., 1969. Mesure de la periode du protactinium-231 par
800 microcalorimetrie. Radiochim. Acta 11, 104-108.

801 Robinson, L.F., Belshaw, N.S., Henderson, G.M., 2004. U and Th concentrations and isotope ratios in
802 modern carbonates and waters from the Bahamas. Geochim. Cosmochim. Acta 68, 1777-1789.

803 Rona, P.A., 1980. TAG Hydrothermal Field: Mid-Atlantic Ridge crest at latitude 26°N. J. Geol. Soc.
804 London 137, 385-402.

805 Rona, P.A., Thompson, G., Mottl, M.J., Karson, J.A., Jenkins, W.J., Graham, D., Mallette, M., Von
806 Damm, K., Edmond, J.M., 1984. Hydrothermal activity at the Trans-Atlantic Geotraverse Hydrothermal
807 Field, Mid-Atlantic Ridge crest at 26°N. J.f Geophys. Res.: Solid Earth 89, 11365-11377.

808 Roy-Barman, M., 2009. Modelling the effect of boundary scavenging on thorium and protactinium
809 profiles in the ocean. Biogeosciences 6, 3091-3197.

810 Rutgers v. d. Loeff, M., Berger, G.W., 1993. Scavenging of ^{230}Th and ^{231}Pa near the Antarctic polar front
811 in the South Atlantic. Deep Sea Res. Pt. I 40, 339-357.

812 Sarmiento, J.L., Simeon, J., Gnanadesikan, A., Gruber, N., Key, R.M., Schlitzer, R., 2007. Deep ocean
813 biogeochemistry of silicic acid and nitrate. Global Biogeochem. Cycles 21, GB1S90.

814 Schlitzer, R., 1987. Renewal rates of East Atlantic deep water estimated by inversion of ^{14}C data. J.
815 Geophys. Res.: Oceans 92, 2953-2969.

816 Schlitzer, R., 2011. http://odv.awi.de.

817 Schlitzer, R., Roether, W., Weidmann, U., Kalt, P., Loosli, H.H., 1985. A meridional ^{14}C and ^{39}Ar section
818 in northeast Atlantic deep water. J. Geophys. Res.: Oceans 90, 6945-6952.

819 Schmidt, S., 2006. Impact of the Mediterranean Outflow Water on particle dynamics in intermediate
820 waters of the Northeast Atlantic, as revealed by ^{234}Th and ^{228}Th. Mar. Chem. 100, 289-298.

821 Scholten, J.C., Fietzke, J., Mangini, A., Garbe-Schönberg, C.D., Eisenhauer, A., Schneider, R., Stoffers,
822 P., 2008. Advection and scavenging: Effects on ^{230}Th and ^{231}Pa distribution off Southwest Africa. Earth
823 Planet. Sci. Lett. 271, 159-169.

824 Scholten, J.C., Fietzke, J., Vogler, S., Rutgers van der Loeff, M.M., Mangini, A., Koeve, W., Waniek, J.,
825 Stoffers, P., Antia, A., Kuss, J., 2001. Trapping efficiencies of sediment traps from the deep Eastern
826 North Atlantic: the ^{230}Th calibration. Deep Sea Res. Pt. II 48, 2383-2408.

827 Shen, C.-C., Cheng, H., Edwards, R.L., Moran, S.B., Edmonds, H.N., Hoff, J.A., Thomas, R.B., 2003.
828 Measurement of Attogram Quantities of ^{231}Pa in Dissolved and Particulate Fractions of Seawater by
829 Isotope Dilution Thermal Ionization Mass Spectroscopy. Anal. Chem. 75, 1075-1079.

830 Shen, C.-C., Lawrence Edwards, R., Cheng, H., Dorale, J.A., Thomas, R.B., Bradley Moran, S.,
831 Weinstein, S.E., Edmonds, H.N., 2002. Uranium and thorium isotopic and concentration measurements
832 by magnetic sector inductively coupled plasma mass spectrometry. Chem. Geol. 185, 165-178.

833 Shen, C.-C., Wu, C.-C., Cheng, H., Lawrence Edwards, R., Hsieh, Y.-T., Gallet, S., Chang, C.-C., Li, T.-
834 Y., Lam, D.D., Kano, A., Hori, M., Spötl, C., 2012. High-precision and high-resolution carbonate ^{230}Th
835 dating by MC-ICP-MS with SEM protocols. Geochim. Cosmochim. Acta 99, 71-86.

836 Shimmield, G.B., Murray, J.W., Thomson, J., Bacon, M.P., Anderson, R.F., Price, N.B., 1986. The
837 distribution and behaviour of ^{230}Th and ^{231}Pa at an ocean margin, Baja California, Mexico. Geochim.
838 Cosmochim. Acta 50, 2499-2507.

839 Siddall, M., Anderson, R.F., Winckler, G., Henderson, G.M., Bradtmiller, L.I., McGee, D., Franzese, A.,
840 Stocker, T.F., Müller, S.A., 2008. Modeling the particle flux effect on distribution of ^{230}Th in the
841 equatorial Pacific. Paleoceanography 23, PA2208.

842 Singh, A.K., Marcantonio, F., Lyle, M., 2013. Water column ^{230}Th systematics in the eastern equatorial
843 Pacific Ocean and implications for sediment focusing. Earth Planet. Sci. Lett. 362, 294-304.

844 Speer, K.G., 1989. a forced baroclinic vortex around a hydrothermal plume. Geophysical Research
845 Letters 16, 461-464.

846 Spencer, D.W., Bacon, M.P., Brewer, P.G., 1981. Models of the distribution of ^{210}Pb in a section across
847 the North Equatorial Atlantic Ocean. J. Mar. Res. 39, 119-138.

848 Suman, D.O., Bacon, M.P., 1989. Variations in Holocene sedimentation in the North American Basin
849 determined from ^{230}Th measurements. Deep Sea Res. Pt. A 36, 869-878.

850 Talley, L.D., 1999. Some aspects of ocean heat transport by the shallow, intermediate and deep
851 overturning circulations, Mechanisms of Global Climate Change at Millenial Time Scales, Geophys.
852 Monogr. Amer. Geophy. Union, pp. 1-22.

853 Talley, L.D., Reid, J.L., Robbins, P.E., 2003. Data-Based Meridional Overturning Streamfunctions for the
854 Global Ocean. J. Clim. 16, 3213-3226.

855 Thorpe, S., 1972. A sediment cloud below the Mediterranean outflow. Nature 239, 326-327.

Toole, J.M., Curry, R.G., Joyce, T.M., McCartney, M., Peña-Molino, B., 2011. Transport of the North Atlantic Deep Western Boundary Current about 39°N, 70°W: 2004–2008. Deep Sea Res. Pt. II 58, 1768-1780.

Tsuchiya, M., 1989. Circulation of the Antarctic Intermediate Water in the North Atlantic Ocean. J. Mar. Res. 47, 747-755.

Turnewitsch, R., Reyss, J.-L., Nycander, J., Waniek, J.J., Lampitt, R.S., 2008. Internal tides and sediment dynamics in the deep sea—Evidence from radioactive $^{234}Th/^{238}U$ disequilibria. Deep Sea Res. Pt. I 55, 1727-1747.

Turnewitsch, R., Springer, B.M., 2001. Do bottom mixed layers influence 234Th dynamics in the abyssal near-bottom water column? Deep Sea Res. Pt. I 48, 1279-1307.

Venchiarutti, C., Jeandel, C., Roy-Barman, M., 2008. Particle dynamics study in the wake of Kerguelen Island using thorium isotopes. Deep Sea Res. Pt. I 55, 1343-1363.

Vogler, S., Scholten, J., Rutgers van der Loeff, M., Mangini, A., 1998. ^{230}Th in the eastern North Atlantic: the importance of water mass ventilation in the balance of ^{230}Th. Earth Planet. Sci. Letters 156, 61-74.

Walter, H.-J., Rutgers v. d. Loeff, M.M., Francois, R., 1999. Reliability of the $^{231}Pa/^{230}Th$ Activity Ratio as a Tracer for Bioproductivity of the Ocean, in: Fischer, W., Wefer, G. (Eds.), Use of Proxies in Paleoceanography: Examples for the South Atlantic. Springer-Verlag, Berlin, pp. 393-408.

Weyer, S., Anbar, A.D., Gerdes, A., Gordon, G.W., Algeo, T.J., Boyle, E.A., 2008. Natural fractionation of $^{238}U/^{235}U$. Geochim. Cosmochim. Acta 72, 345-359.

Wunsch, C., Heimbach, P., 2006. Estimated Decadal Changes in the North Atlantic Meridional Overturning Circulation and Heat Flux 1993–2004. J. Phys. Oceanogr. 36, 2012-2024.

Wunsch, C., Heimbach, P., 2013. Two Decades of the Atlantic Meridional Overturning Circulation: Anatomy, Variations, Extremes, Prediction, and Overcoming Its Limitations. J. Climate 26, 7167-7186.

Yang, H.-S., Nozaki, Y., Sakai, H., Masuda, A., 1986. The distribution of ^{230}Th and ^{231}Pa in the deep-sea surface sediments of the Pacific Ocean. Geochim. Cosmochim. Acta 50, 81-89.

Yu, E.-F., Francois, R., Bacon, M.P., 1996. Similar rates of modern and last-glacial ocean thermohaline circulation inferred from radiochemical data. Nature 379, 689-694.

Yu, E.-F., Francois, R., Bacon, M.P., Fleer, A.P., 2001. Fluxes of ^{230}Th and ^{231}Pa to the deep sea: implications for the interpretation of excess ^{230}Th and $^{231}Pa/^{230}Th$ profiles in sediments. Earth Planet. Sci. Lett. 191, 219-230.

Zenk, W., Klein, B., Schroder, M., 1991. Cape Verde Frontal Zone. Deep Sea Res. Pt. A 38, Supplement 1, S505-S530.

888
889

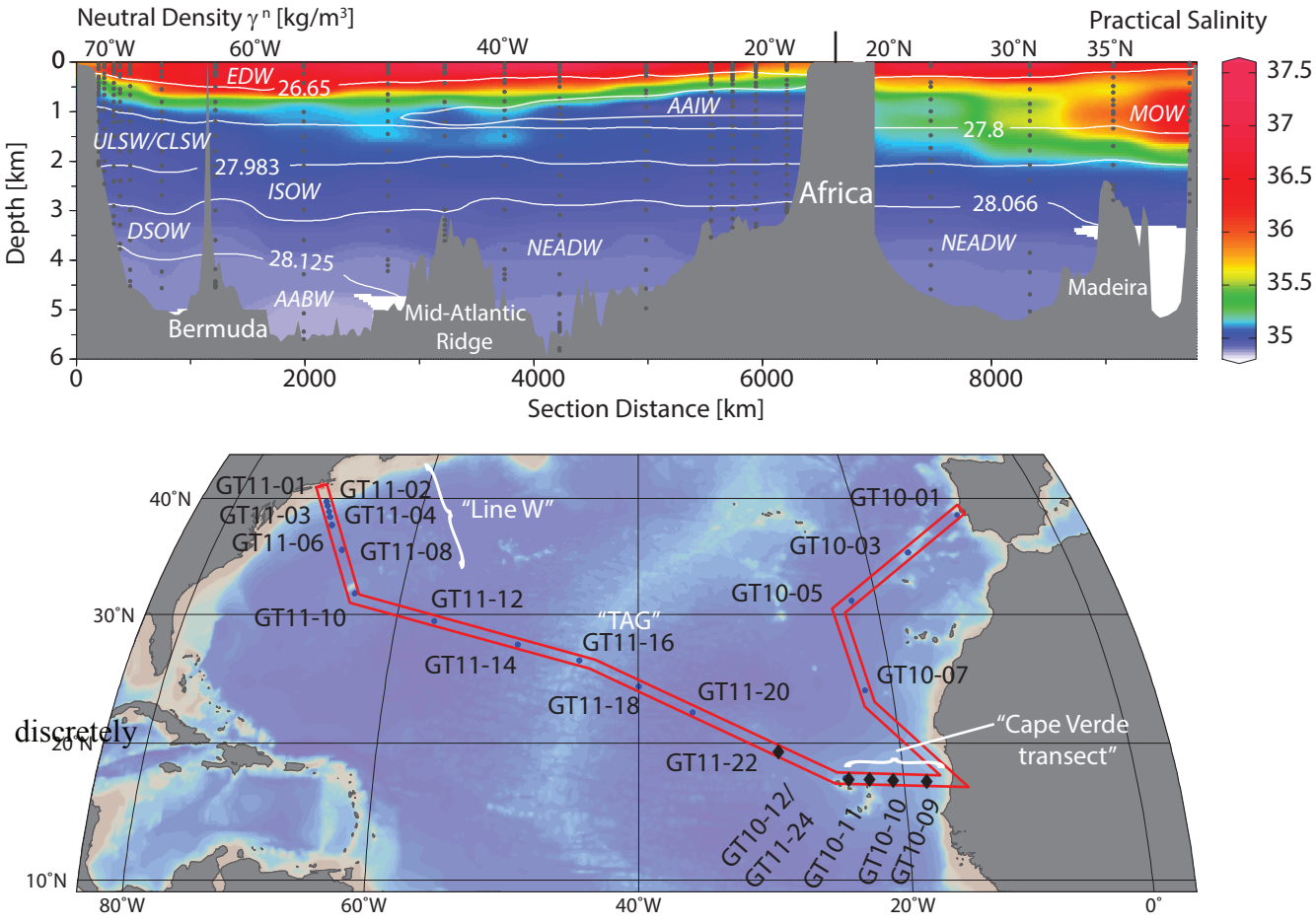

discretely

Figure 1

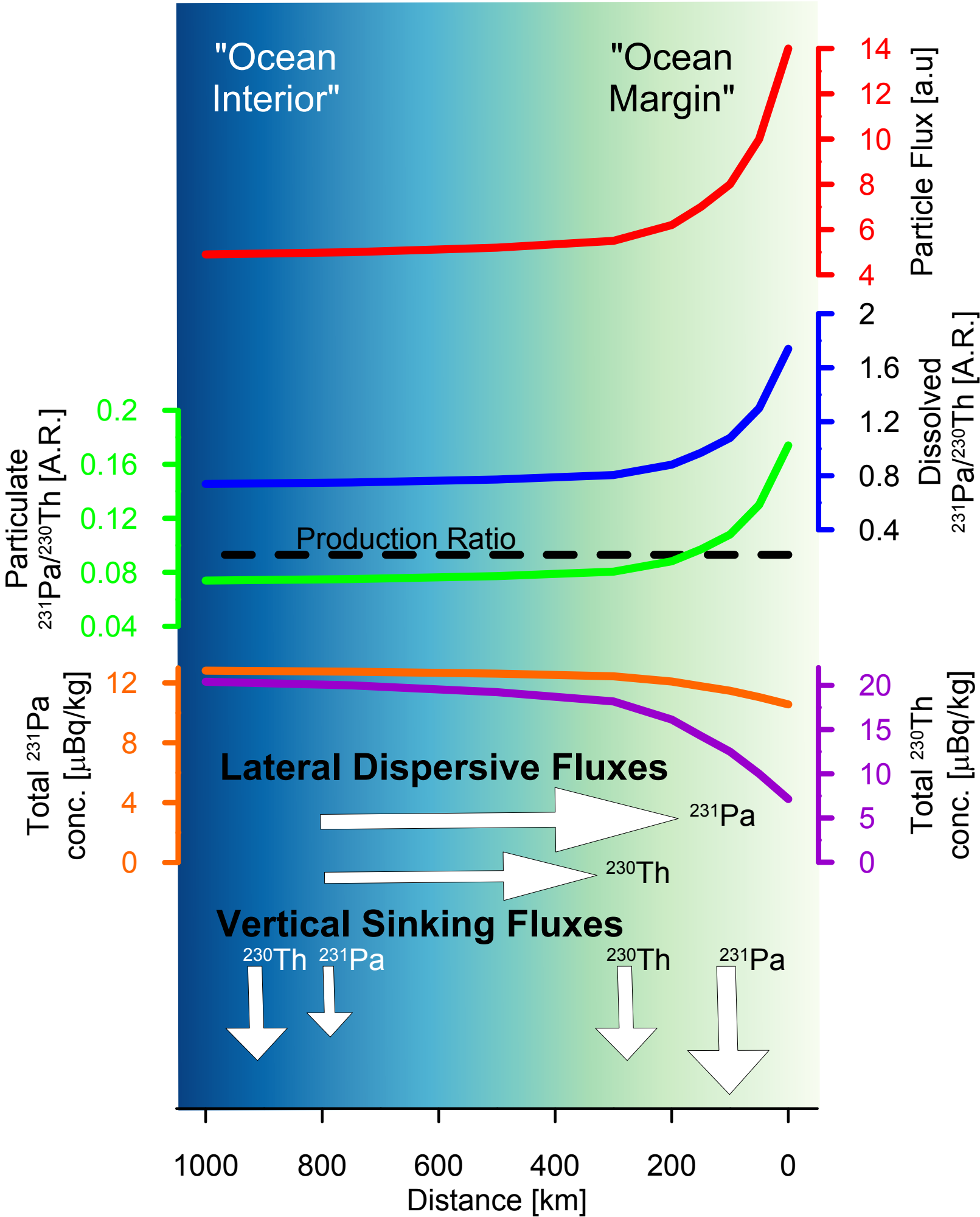
"Ocean Interior"
"Ocean Margin"
Particle Flux [a.u]
14
12
10
8
6
4
Dissolved $^{231}Pa/^{230}Th$ [A.R.]
2
1.6
1.2
0.8
0.4
Production Ratio
Particulate $^{231}Pa/^{230}Th$ [A.R.]
0.2
0.16
0.12
0.08
0.04
Total ^{231}Pa conc. [µBq/kg]
12
8
4
0
Total ^{230}Th conc. [µBq/kg]
20
15
10
5
0
Lateral Dispersive Fluxes
^{231}Pa
^{230}Th
Vertical Sinking Fluxes
^{230}Th
^{231}Pa
^{230}Th
^{231}Pa
1000
800
600
400
200
0
Distance [km]

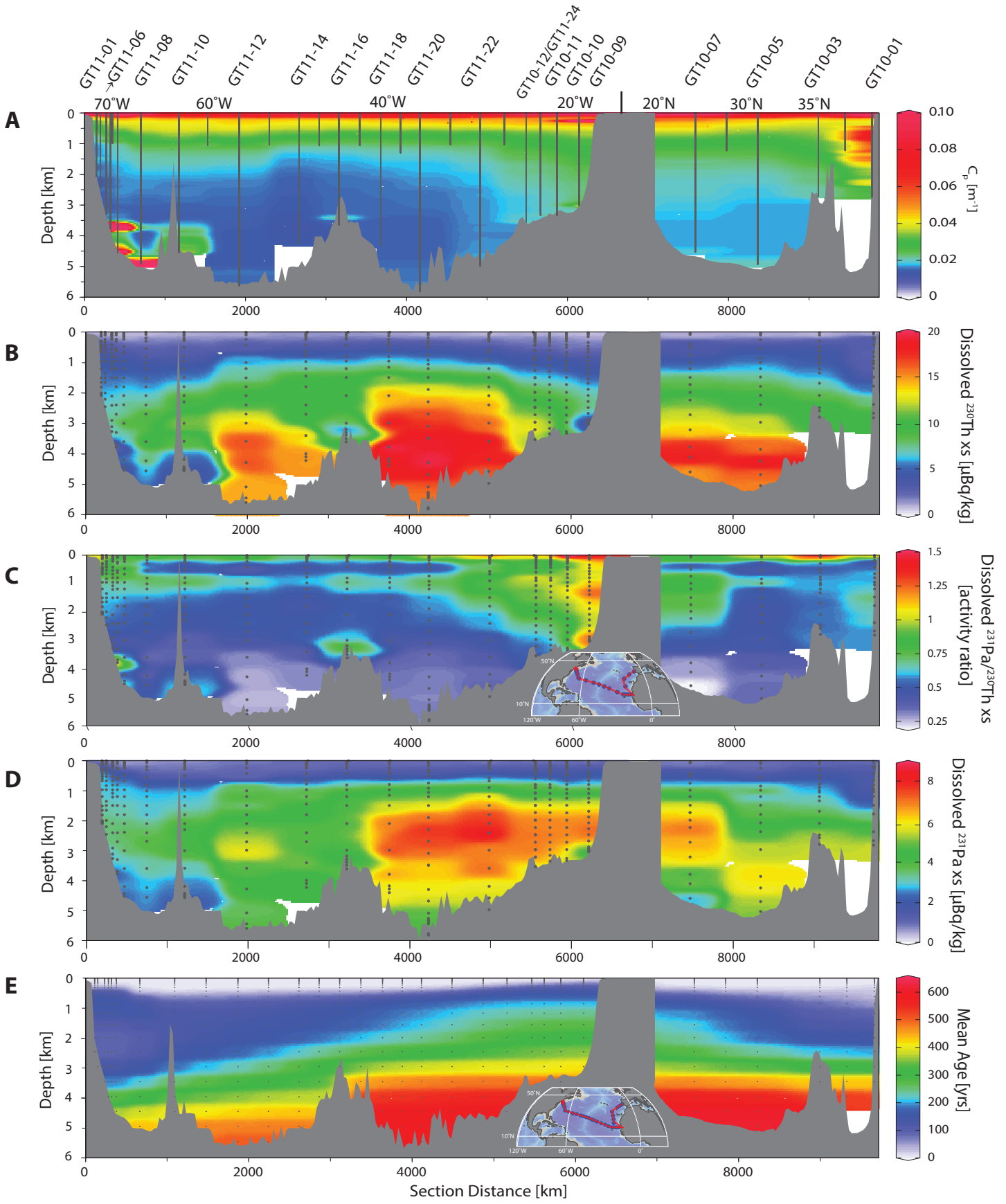
GT11-01
GT11-06
GT11-08
GT11-10
GT11-12
GT11-14
GT11-16
GT11-18
GT11-20
GT11-22
GT10-12/GT11-24
GT10-11
GT10-10
GT10-09
GT10-07
GT10-05
GT10-03
GT10-01
70°W
60°W
40°W
20°W
20°N
30°N
35°N
A
B
C
D
E
Depth [km]
Section Distance [km]
C_p [m^{-1}]
Dissolved ^{230}Th xs [µBq/kg]
Dissolved ^{231}Pa/^{230}Th xs [activity ratio]
Dissolved ^{231}Pa xs [µBq/kg]
Mean Age [yrs]

Figure 3.

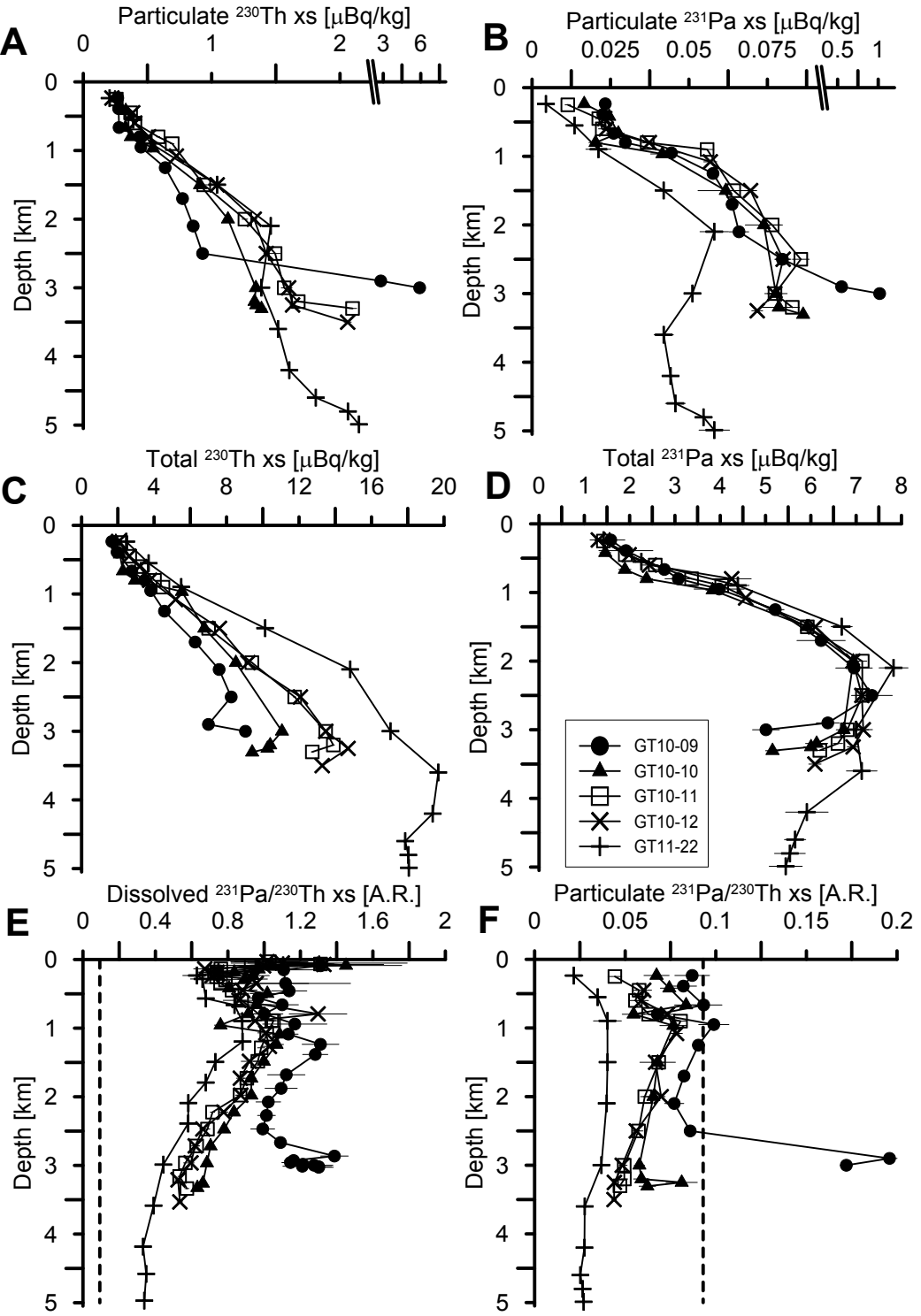
A
Particulate 230Th xs [μBq/kg]
0
1
2
3
6
B
Particulate 231Pa xs [μBq/kg]
0
0.025
0.05
0.075
0.5
1
C
Total 230Th xs [μBq/kg]
0
4
8
12
16
20
D
Total 231Pa xs [μBq/kg]
0
1
2
3
4
5
6
7
8
E
Dissolved 231Pa/230Th xs [A.R.]
0
0.4
0.8
1.2
1.6
2
F
Particulate 231Pa/230Th xs [A.R.]
0
0.05
0.1
0.15
0.2
Depth [km]
0
1
2
3
4
5
GT10-09
GT10-10
GT10-11
GT10-12
GT11-22

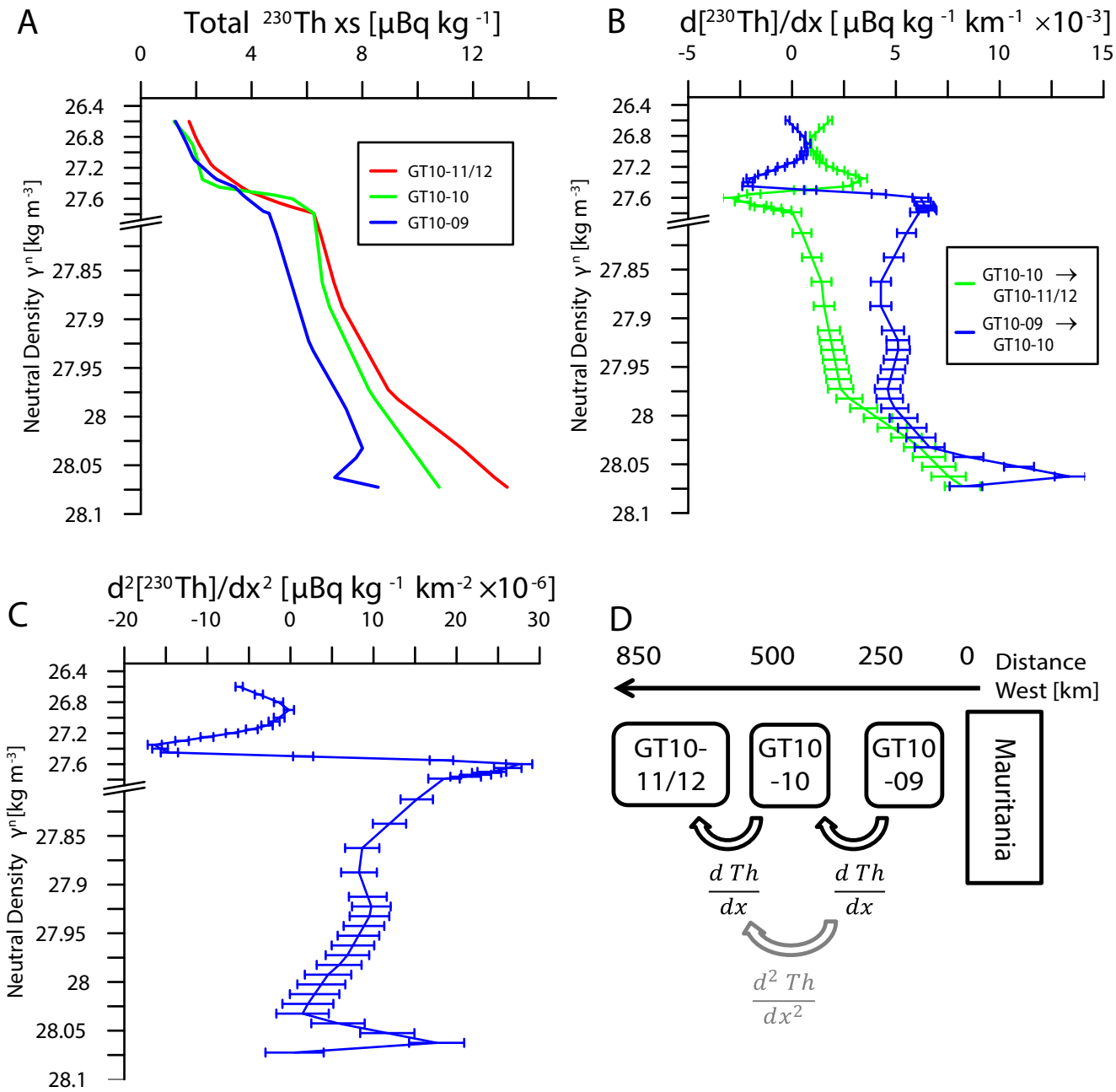
A
Total ^{230}Th xs [µBq kg^{-1}]
0
4
8
12
Neutral Density γ^n [kg m^{-3}]
26.4
26.8
27.2
27.6
27.85
27.9
27.95
28
28.05
28.1
GT10-11/12
GT10-10
GT10-09
B
d[^{230}Th]/dx [µBq kg^{-1} km^{-1} ×10^{-3}]
-5
0
5
10
15
GT10-10 → GT10-11/12
GT10-09 → GT10-10
C
d^2[^{230}Th]/dx^2 [µBq kg^{-1} km^{-2} ×10^{-6}]
-20
-10
0
10
20
30
D
850
500
250
0
Distance West [km]
GT10-11/12
GT10-10
GT10-09
Mauritania
$\frac{d\,Th}{dx}$
$\frac{d\,Th}{dx}$
$\frac{d^2\,Th}{dx^2}$

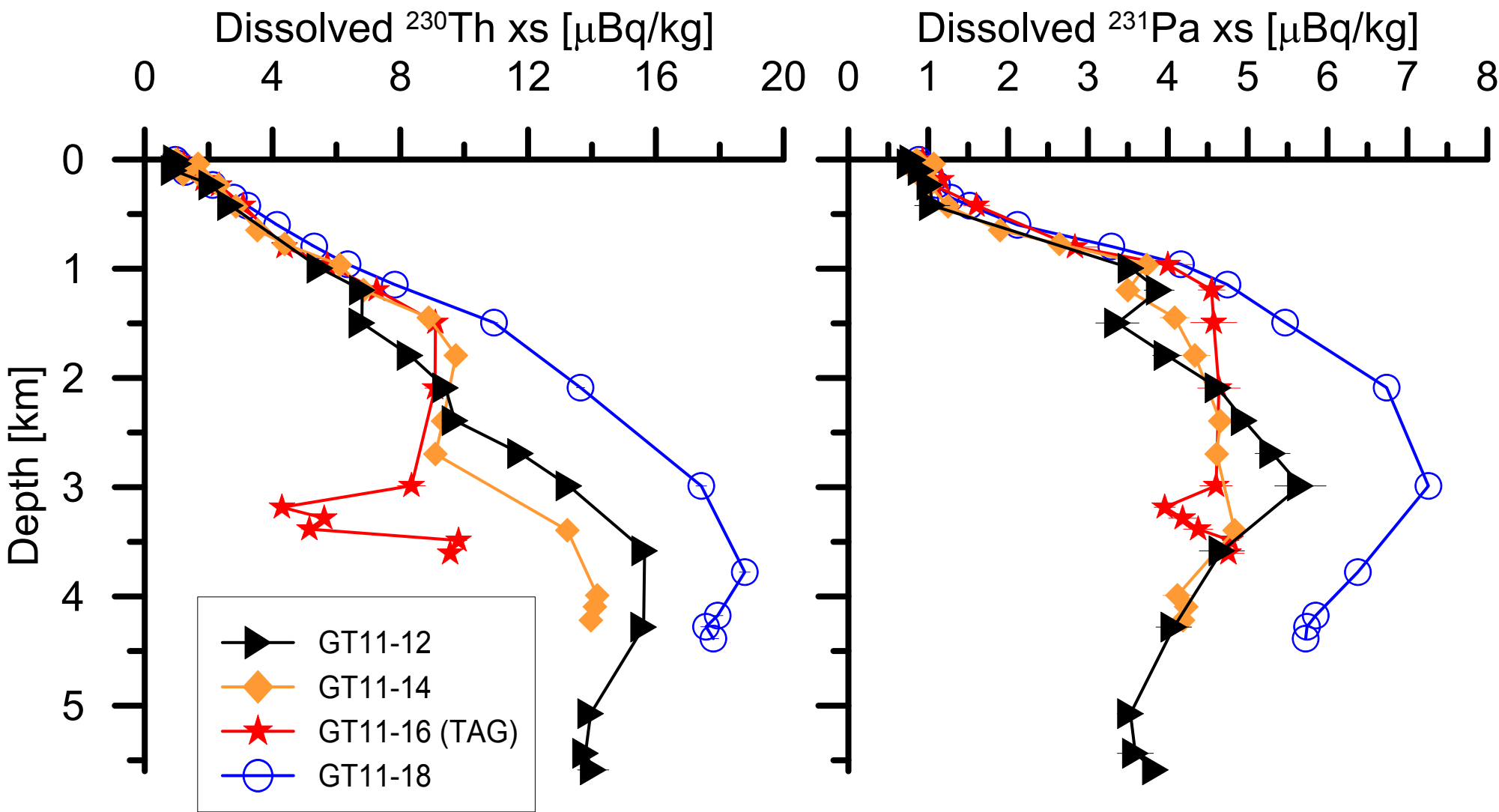
Dissolved ^{230}Th xs [μBq/kg]
0
4
8
12
16
20
Dissolved ^{231}Pa xs [μBq/kg]
0
1
2
3
4
5
6
7
8
Depth [km]
0
1
2
3
4
5
GT11-12
GT11-14
GT11-16 (TAG)
GT11-18

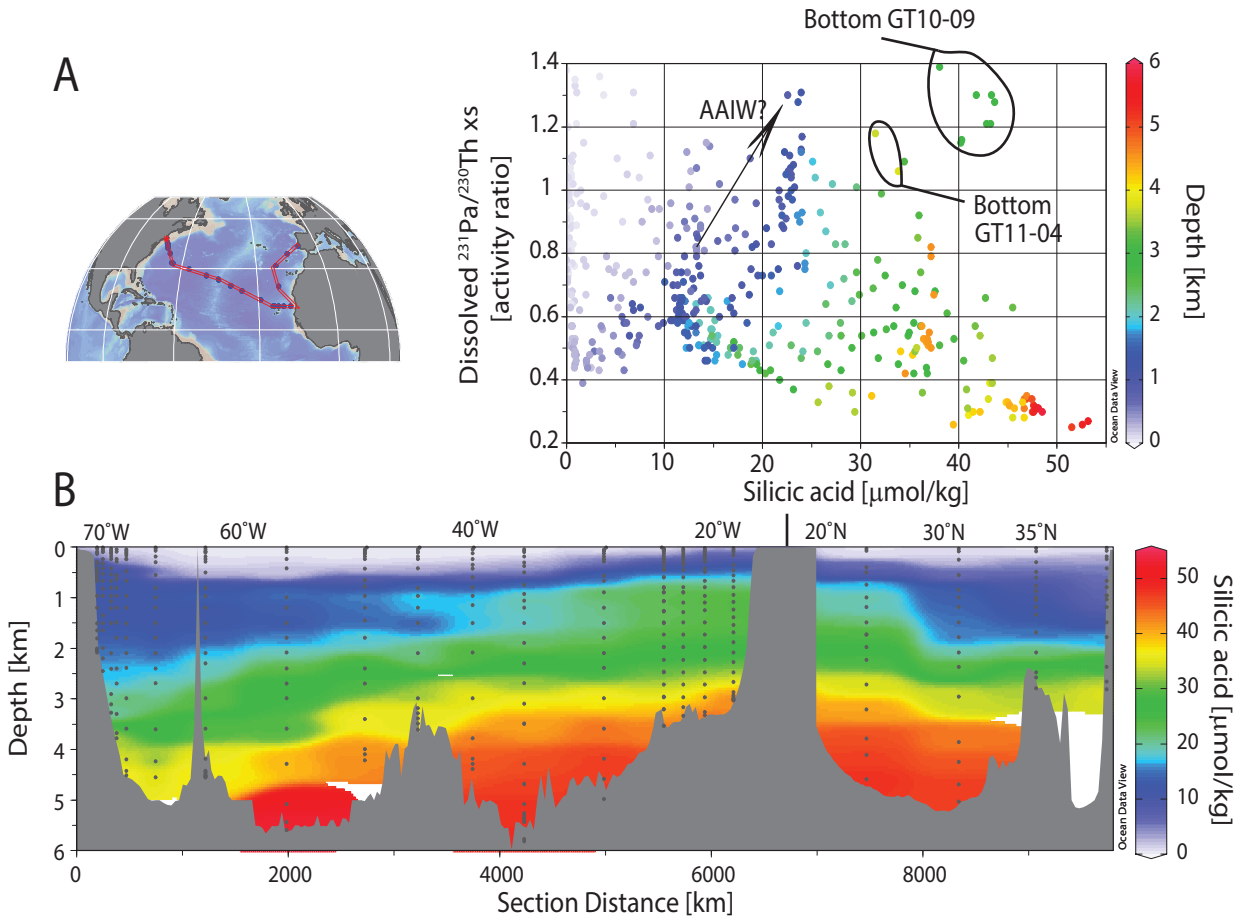
A
Bottom GT10-09
AAIW?
Bottom
GT11-04
Dissolved ^{231}Pa/^{230}Th xs
[activity ratio]
Silicic acid [µmol/kg]
Depth [km]
Ocean Data View
B
70°W
60°W
40°W
20°W
20°N
30°N
35°N
Depth [km]
Section Distance [km]
Silicic acid [µmol/kg]
Ocean Data View

Figure 7.